https://doi.org/10.5194/egusphere-2026-4080
Preprint. Discussion started: 21 July 2026


# Modelling eddy diffusivity in the ocean with scalar-velocity cospectra

Achim Randelhoff[1]

[1]Akvaplan-niva, Fram Centre, Tromsø, Norway

**Correspondence:** Achim Randelhoff (ara@akvaplan.niva.no)

**Abstract.** This paper outlines a pathway to understanding eddy diffusivity in stratified flows by considering scalar-velocity cospectra, also called scalar flux spectra ($\mathrm{E}_{\mathrm{w}\theta}$). Its main objective is to unify existing scalings of eddy diffusivity into a quantitative recipe. We construct a synthetic model scalar-velocity cospectrum for stratified turbulence applicable to the ocean. Its integral over all wavenumbers, normalized by the mean scalar gradient, equals eddy diffusivity and scales principally with horizontal Froude number $\mathrm{Fr}_h$ and buoyancy Reynolds number $\mathrm{Re}_\mathrm{b}$. Our model spectrum reproduces published mixing coefficient estimates from oceanic microstructure and direct numerical simulation (DNS), as well as a new analysis of existing eddy covariance data, over the entire accessible range of $\mathrm{Fr}_h$, or equivalently, Ozmidov/Thorpe length scale ratios. However, scaling between eddy diffusivities and $\mathrm{Fr}_h$ for strongly stratified flows, $\mathrm{Fr}_h < 1$, appears to differ between most DNS and oceanic measurements. We particularly emphasize the importance of the spectral slope $s_b$ between the Ozmidov and integral length scales, finding best agreement with ocean observations when assuming $s_b \approx -4/3$, but $s_b \approx 1/3$ for DNS for the stratified wavenumber range. We argue that this difference may be due to the length scale of the forcing. From direct measurements of scalar-velocity cospectra in the ice-ocean boundary layer, we find that additional contributions to eddy diffusivity at low Froude numbers may result from background processes not scaling with $\mathrm{Fr}_h$ or $\mathrm{Re}_\mathrm{b}$, which warrants further investigation into boundary layer processes.

## 1 Introduction

Turbulent mixing is a key factor determining the oceanic environment, from global energetic considerations through water mass transformations to small-scale phytoplankton blooms (Lewis et al., 1986; Munk and Wunsch, 1998). Vertical fluxes $F_\theta$ of a tracer $\theta$ in the ocean are routinely calculated from turbulence kinetic energy dissipation $\epsilon$ by assuming[1]: First, the existence of an eddy diffusivity

$$K_\theta = -F_\theta / G \tag{1}$$

for any tracer $\theta$ such as temperature $T$, salinity $S$ or density $\rho$ (equivalently, buoyancy $b$), where $G$ is the mean scalar vertical gradient of the tracer in question. Second, a relation of the form

$$K_\rho \approx \Gamma \epsilon / N^2, \tag{2}$$

[1]See also the glossary in Appendix C

https://doi.org/10.5194/egusphere-2026-4080
Preprint. Discussion started: 21 July 2026


first proposed as an upper bound by Osborn (1980), where $K_\rho$ is the vertical eddy diffusivity of density, $N \equiv \sqrt{-g/\rho_0\,\partial\rho/\partial z}$ the buoyancy frequency, $g$ the gravitational acceleration, $\rho_0$ a reference density, and we term $\Gamma$ the mixing coefficient. Third, one assumes Eq. 2 to apply to eddy diffusivity $K_\theta$ of any tracer $\theta$ by invoking Reynolds analogy for fully developed turbulence, i.e., $K_\rho = K_\theta$. The fourth and final assumption is that $\Gamma$ can be approximated using a constant value, in general taken to be $\Gamma \approx 0.2$. This brushes over multiple potential sources of variability, both from general oceanic processes and specific to a given mixing event (Caulfield, 2020; Mashayek et al., 2021). As Gregg et al. (2018) highlighted, while most studies agree about the existence of such variability, the recommended $\Gamma \approx 0.2$ value largely reflects the fact that there currently is no alternative parameterization with sufficient support.

An additional complication is the existence of multiple definitions of $\Gamma$ relating to exactly which quantity denotes mixing. Following Caulfield (2020), we define

$$\Gamma \equiv -\frac{F_b}{\epsilon} \tag{3}$$

with the buoyancy flux $F_b$. With further assumptions on the buoyancy conservation equation (such as steady state, non-divergence of transport terms), one can approximate $\Gamma$ using one of several expressions for mixing. The rate of *irreversible* mixing $\mathcal{M}$ represents the increase in background potential energy (e.g., Winters et al., 1995; Caulfield and Peltier, 2000), leading to $\Gamma_\mathcal{M} \equiv \frac{\mathcal{M}}{\epsilon}$ (Peltier and Caulfield, 2003). The rate of buoyancy dissipation $\epsilon_b$, i.e. $\Gamma_\chi \equiv \frac{\epsilon_b}{N^2\epsilon}$ (Oakey, 1982; Caulfield, 2020), is equal to the buoyancy flux $F_b$ only in steady state and in the absence of transport terms in the buoyancy variance conservation equation. One then usually arrives at the approximations $\Gamma \simeq \Gamma_\mathcal{M} \simeq \Gamma_\chi$ necessary for comparing data from different sources, which we will apply throughout this paper.

In this paper, we explore a different approach: Instead of estimating $K_\theta$ from $\Gamma$, we directly consider the nondimensional eddy diffusivity

$$\tilde{K}_\theta \equiv K_\theta \frac{N^2}{\epsilon} \tag{4}$$

for any tracer $\theta$ which may or may not be density. (Note that we choose non-dimensionalising $K_\theta$ with $\epsilon/N^2$ for easier comparison with an Osborn-style formula. Non-dimensionalising with a mixing-length type eddy diffusivity (the product of a length and a velocity scale) is of course possible but complicates isolating the effects of stratification as will become clearer below.) To this end, we use the scalar-velocity cospectrum $\mathrm{E}_{\mathrm{w}\theta}$ (also called flux spectrum) between a tracer $\theta$ and (vertical) velocity $w$. By definition, $\mathrm{E}_{\mathrm{w}\theta}$ integrates to $\int_0^\infty \mathrm{d}k\,\mathrm{E}_{\mathrm{w}\theta} = F_\theta$, with $k$ the wavenumber, which yields a parameterization

$$\tilde{K}_\theta = -\int_0^\infty \mathrm{d}k\,\frac{\mathrm{E}_{\mathrm{w}\theta} N^2}{\epsilon G} \tag{5}$$

with the mean scalar gradient $G$. Eq. 4 of course resembles the definition of $\Gamma$, and by practical necessity we will indeed rely on experimental estimates of $\Gamma$ and implicitly make the assumptions necessary for approximating $\tilde{K}_\theta \approx \Gamma$ to evaluate our approach. However, we stress that the model presented herein explicitly computes $\tilde{K}_\theta$, not its approximation via $\Gamma$. We will write $\tilde{K}_\rho$ whenever we specifically address the diffusivity for density and otherwise use the more generic $\tilde{K}_\theta$.

https://doi.org/10.5194/egusphere-2026-4080
Preprint. Discussion started: 21 July 2026


In Sec. 2, we will substantiate Eq. 5 by constructing a synthetic model spectrum for stratified turbulence that can be used for quantitative computations of $\tilde{K}_\theta$. In Sec. 3, we will present data sets from DNS (Direct Numerical Simulation) as well as the ocean both from microstructure (ocean interior) and eddy covariance (from the ice-ocean boundary layer). Finally, in Sec. 4, we will evaluate the resulting model for $\tilde{K}_\theta$ with available data, and formulate some conclusions and questions for future work in Sec. 5.

## 2 A model spectrum for stratified turbulence with a scalar mean gradient

### 2.1 Motivation and basic definitions

We start by considering an arbitrary passive tracer $\theta$ with Prandtl number $\mathrm{Pr} = \nu/\kappa_\theta \gtrsim 1$ in isotropic, homogeneous turbulence, where $\kappa_\theta$ is the molecular diffusivity of $\theta$ and $\nu$ the molecular viscosity of seawater. (In the ocean, $\mathrm{Pr} \approx 7$ for temperature; when salinity is the tracer, the corresponding Schmidt number $\mathrm{Sc} = \nu/\kappa_\theta \approx 700$. Many authors cited herein use "Schmidt number" throughout, even for temperature.)

We define three length scales besides the integral length scale of the flow, $\ell$, and a turbulent velocity scale $U$: First, the Kolmogorov length $\eta = (\nu^3/\epsilon)^{1/4}$, below which turbulent kinetic energy K is dissipated at rate $\epsilon$. Second, the Batchelor length scale $\eta_B \equiv \eta/\sqrt{\mathrm{Pr}}$, below which variance of tracer $\theta$ is dissipated. Third, the Ozmidov length $\ell_O = (\epsilon/N^3)^{1/2}$, the largest length scale that has enough turbulent energy to overturn. These length scales define the four spectral ranges to be considered for $\mathrm{E}_{\mathrm{w}\theta}$ in wavenumber ($k$) space: The large scales ($k \ll 1/\ell$), the stratified range ($1/\ell \ll k \ll 1/\ell_O$, only for $\mathrm{Fr}_h \ll 1$), the inertial-convective range ($1/\ell_O \ll k \ll 1/\eta$ or, for $\mathrm{Fr} \geq 1$, $1/\ell \ll k \ll 1/\eta$), and the viscous range ($1/\eta \ll k$). For simplicity, we omit separating the viscous-convective and viscous-diffusive ranges ($1/\eta_B \ll k$) as the rolloff is already exponential starting at $\eta$ and hence this region of the cospectrum contributes very little to the integral (see Appendix A).

From these length scales we further construct the Reynolds number $\mathrm{Re} \equiv (\ell/\eta)^{4/3}$ and the buoyancy Reynolds number $\mathrm{Re_b} \equiv (\ell_O/\eta)^{4/3} = \epsilon/(\nu N^2)$. Then we can define the Froude number $\mathrm{Fr} \equiv (\mathrm{Re_b}/\mathrm{Re})^{1/2} = (\ell_O/\ell)^{2/3}$. Assuming the Taylor scaling $\epsilon \simeq U^3/\ell$, this definition of the Froude number is equivalent to two well-known ones: as $\mathrm{Fr} = U/(N\ell)$, the relation of the turbulent timescale ($\ell$/$U$) to the buoyancy time scale (1/$N$), and $\mathrm{Fr} = \epsilon/(N\mathrm{K})$, constructed from turbulent kinetic energy K and $\epsilon$; it also recovers the common definition $\mathrm{Re} = U\ell/\nu$. In the unstratified case, $N \to 0^+$ and $\mathrm{Fr} \to +\infty$ by definition. In summary,

$$\begin{aligned}
\mathrm{Re} &= \mathrm{Fr}^{-2}\mathrm{Re_b} \\
(\ell/\eta)^{4/3} &= (\ell/\ell_O)^{4/3}(\ell_O/\eta)^{4/3}. \qquad (6)
\end{aligned}$$

Crucially, Eq. 6 supposes the Taylor scaling, which however has good support for both unstratified and stratified flows as discussed below.

On dimensional grounds, Lumley (1964) proposed the (unstratified) scalar-velocity cospectrum

$$\mathrm{E}_{\mathrm{w}\theta} = -\mathrm{C}_{\mathrm{w}\theta} G \epsilon^{1/3} k^{-7/3} \qquad (7)$$

https://doi.org/10.5194/egusphere-2026-4080
Preprint. Discussion started: 21 July 2026


for the inertial-convective subrange $1/\ell \ll k \ll 1/\eta$, where $\mathrm{C}_{\mathrm{w}\theta}$ is an $\mathcal{O}(1)$ constant and $G$ the scalar mean gradient of any tracer $\theta$. Over the inertial-convective subrange, which for $\mathrm{Fr} \geq 1 \Leftrightarrow \ell \leq \ell_O$ we can assume extends to $\ell$, Eq. 7 integrates to

$$-\frac{G\epsilon}{N^2}\tilde{K}_\theta = F_\theta \approx \int_{1/\ell}^{1/\eta} \mathrm{d}k\,\mathrm{E}_{\mathrm{w}\theta} = -\frac{3}{4}\mathrm{C}_{\mathrm{w}\theta} G \epsilon^{1/3}\left(\ell^{4/3} - \eta^{4/3}\right), \tag{8}$$

which determines the functional form and provides the bulk of the contribution to $\tilde{K}_\theta$. In Appendix A, we demonstrate that contributions from scales larger than $\ell$ and smaller than $\eta$ likely do not contribute much to $\tilde{K}_\theta$ except in the case $\ell \to \eta$ and, more importantly, do not change the functional form beyond modifying the prefactors of the $\ell^{4/3}$ and $\eta^{4/3}$ terms.

Dividing Eq. 8 by $-G\epsilon/N^2 = -G\epsilon^{1/3}\ell_O^{4/3}$ and for now neglecting the contributions of the large scales and the viscous subrange, we obtain:

$$\tilde{K}_\theta \approx \frac{3}{4}\mathrm{C}_{\mathrm{w}\theta}\left(\frac{1}{\mathrm{Fr}^2} - \frac{1}{\mathrm{Re_b}}\right) \qquad \text{for } \mathrm{Fr} > 1,\ \mathrm{Re_b} > 1 \tag{9}$$

At first glance, Eq. 9 reproduces the scalings reported in the literature based on numerical, laboratory and field experiments as well as on dimensional grounds in two crucial aspects: The suppression of vertical mixing for $\mathrm{Re_b} \sim \mathcal{O}(10)$ (Ivey and Imberger, 1991; Bouffard and Boegman, 2013) and the $\Gamma \sim \mathrm{Fr}^{-2}$ scaling for high Fr (Ivey and Imberger, 1991; Garanaik and Venayagamoorthy, 2019).

### 2.2 Extension to stratified flows

Up to here, we have worked with isotropic turbulence in the inertial-convective range, which is relatively unambiguous and well-researched. In other words, for $\mathrm{Fr} > 1$, i.e. weak stratification, $\ell_O > \ell$ and the outer scale of the turbulence does presumably not "feel" $\ell_O$. In the presence of strong vertical density stratification however, the flow becomes anisotropic at length scales above the Ozmidov length $\ell_O$, which we will refer to as the stratified wavenumber range. This means that for $\mathrm{Fr} < 1$, $\ell_O < \ell$, and $\ell_O$ likely plays a determining role, with $\mathrm{E}_{\mathrm{w}\theta}$ taking different forms on each side of $\ell_O$ (Fig. 1). Since turbulent mixing of tracers happens at the large-scale end of the inertial subrange, it can already be guessed from this representation that Fr will play a prominent role in determining $\tilde{K}_\theta$.

Length scales are then different for horizontal and vertical motions, denoted by $\ell_h$ and $\ell_v$, and accordingly the horizontal and vertical Froude numbers $\mathrm{Fr}_h = \frac{U}{\ell_h N}$ and $\mathrm{Fr}_v = \frac{U}{\ell_v N}$. The velocity scale $U$ now represents the largest structures of horizontal motions. Nature invariably seems to prefer $\mathrm{Fr}_v \sim \mathcal{O}(1)$, whereas $\mathrm{Fr}_h$ can vary over orders of magnitude (Riley and Lindborg, 2012, and references therein). Crucially, adapted to these definitions, the modified Taylor scaling $\epsilon \sim U^3/\ell_h$ has good support from DNS (Riley and Lindborg, 2012; Maffioli and Davidson, 2016), and hence we can keep relying on our earlier definitions of Re, $\mathrm{Re_b}$, and Fr (see Eq. 6). In the data sources used below, often the scaling $\mathrm{Fr} = \epsilon/(N\mathrm{K})$ is used. This conveniently represents $\mathrm{Fr}_h$ rather than $\mathrm{Fr}_v$ due to the anisotropy in K, which in the stratified case is dominated by horizontal motions. Hence, we will use $\mathrm{Fr}_h \equiv (\mathrm{Re_b}/\mathrm{Re})^{1/2} = \epsilon/(N\mathrm{K}) = U/(N\ell_h)$ with $\mathrm{Re} = U\ell_h/\nu$ interchangeably.

Note that modelling $K_\rho$ necessarily implies $G \equiv N^2$, but modelling $K_\theta$ of a passive tracer can be done for both stratified ($N^2 > 0$) and unstratified ($N^2 = 0$) flow with no bearing on $G$.

https://doi.org/10.5194/egusphere-2026-4080
Preprint. Discussion started: 21 July 2026


As far as $E_{w\theta}$ is concerned, we will represent stratification by simply changing the spectral slope in the wavenumber range between $\ell_O$ and $\ell_h$. Note that $E_{w\theta}$ represents a shell-summed cospectrum, which now (in the stratified case) results from integration over wavenumber shells of the full anisotropic spectrum. The mere use of a shell-summed cospectrum does hence not strictly imply isotropy; any spectral slope assigned to the stratified wave number range is only an effective value integrating over spectral slopes that vary between the horizontal and vertical directions (Riley and Lindborg, 2012). The justification for this procedure will lie in its success at describing field and DNS observations. Which spectral slope to use for the stratified range will be discussed below.

### 2.3 Construction

In this section, we construct a synthetic model spectrum $E_{w\theta}/G$ from the input values $\mathrm{Re_b}$ and $\mathrm{Fr}_h$ based on multiple parameters: $C_{w\theta}$; the spectral slopes $s_a$, $s_b$, and $s_c$ for the large, stratified, and inertial-convective scales, respectively; $\beta$ the exponential rolloff in the viscous subrange (see Appendix A); and lastly, an empirical flattening factor $\varphi$ (see below). By integrating this spectrum, we then recover a parameterized version of $\tilde{K}_\theta$. The parameter values are discussed in the next subsection.

The synthetic spectrum is constructed as follows: All wavenumbers are scaled with the Kolmogorov length as $k\eta$. From $\mathrm{Re_b}$ and $\mathrm{Fr}_h$, we calculate $\mathrm{Re} = \mathrm{Re_b}/\mathrm{Fr}_h^2$ and $\mathrm{Re}_* = \min(\mathrm{Re}, \mathrm{Re_b})$. $k\eta$ is then $(k\eta)_\ell = \mathrm{Re}^{-3/4} k\eta$ at the integral scale, and $(k\eta)_* = \mathrm{Re}_*^{-3/4} k\eta$ at the Ozmidov or integral scale if $\mathrm{Fr}_h$ smaller or larger than 1, respectively. The inertial-convective range $E_{w\theta}/G = C_{w\theta}\epsilon^{1/3}(k\eta)^{s_c}(k\eta)_*^{-7/3-s_c}\eta^{7/3}$ is set first, extending from $(k\eta)_*$ to 1.

In the high wavenumbers, construction differs depending on the Prandtl number. For $\mathrm{Pr} \geq 1$, we join the viscous-convective subrange ($1/\eta < k < 1/\eta_B$), where $E_{w\theta} \sim \exp(-\beta k\eta/2)$. This spectral form is the maximum inferred from the cospectrum inequality (O'Gorman and Pullin, 2005), see Eq. A1. The parameter $\beta$ describes the viscous rolloff in the turbulent kinetic energy spectrum, $E_u \sim \exp(-\beta k\eta)$. The case $\mathrm{Pr} < 1$ is not relevant for the ocean. However, below, we will compare the DNS by Shih et al. (2005) at $\mathrm{Pr} = 0.72$, corresponding to thermally stratified air. This can be accommodated by inserting an inertial-diffusive range ($\sqrt{\mathrm{Pr}}/\eta \equiv 1/\eta_B < k < 1/\eta$) with spectral slope $-11/3$ (O'Gorman and Pullin, 2005). In practice, this will not significantly change modelled values of $\tilde{K}_\theta$ as this Prandtl number is so close to unity and its spectral slope is so close to the inertial-convective one.

In the stratified subrange $E_{w\theta} \sim k^{s_b}$ (if $\mathrm{Fr}_h$<1) from $(k\eta)_\ell$ to $(k\eta)_*$, and the large scales $E_{w\theta} \sim k^{s_a}$ below $(k\eta)_\ell$ are joined, ensuring continuity.

The spectrum so far assumes a constant spectral slope all the way to $1/\ell_h$ (for $\mathrm{Fr}_h > 1$) or $1/\ell_O$ (for $\mathrm{Fr}_h < 1$). In reality, this peak is of course flattened (Chasnov, 1994). As we will show below, this flattening matters when integrating over all wavenumbers, because it changes the absolute value (not the scaling) of computed $\tilde{K}_\theta$ values. We will refrain from a literature survey on other, possibly more realistic spectral forms in those transition regions. Instead, we simply define the parameter $\varphi \geq 1$ to emulate this flattening (see Fig. 1). Essentially, we smooth the piecewise exponential spectrum in log-log-space using a Hanning window with a window size the width of the wavenumber band $k\eta/\varphi \leq k \leq k\eta\varphi$, then replace the spectral values in the bands $k\eta/\varphi \leq k \leq k\eta\varphi$ around the peaks $1/\ell$ or $1/\ell_O$ (if present) using a tapered version of the smoothed spectrum (tapering again with the same Hanning window).

https://doi.org/10.5194/egusphere-2026-4080
Preprint. Discussion started: 21 July 2026


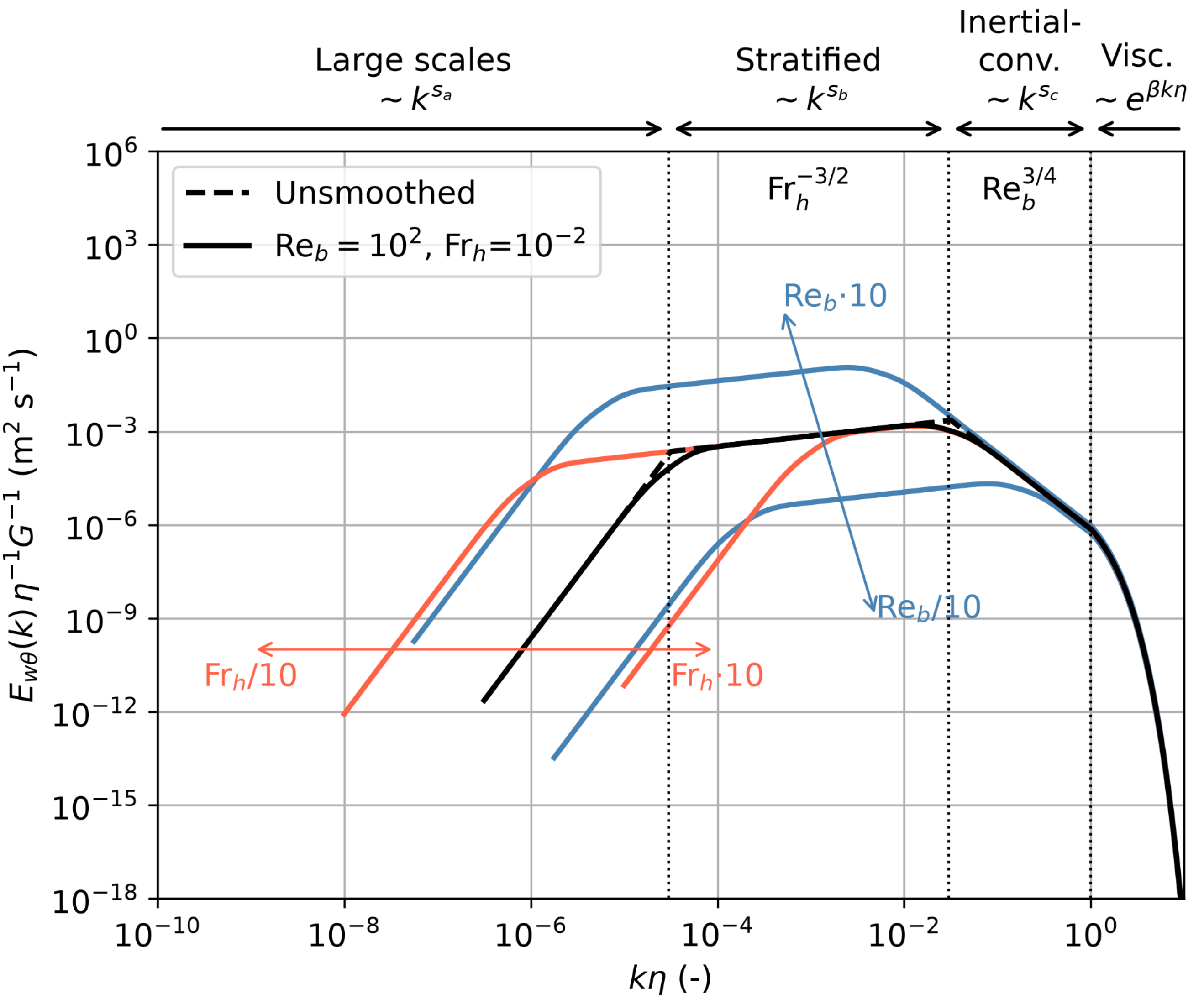


**Figure 1.** Model spectra of $E_{w\theta}$ for $Fr_h$ varying from $10^{-3}$ to $10^{-1}$ and $Re_b$ from $10^1$ to $10^3$. The smoothed spectrum (from $k\eta/10$ to $10k\eta$ around bends) emulates a more realistic spectrum with flattened peaks, important for setting the absolute magnitude of $\tilde{K}_\theta$ (see text).

https://doi.org/10.5194/egusphere-2026-4080
Preprint. Discussion started: 21 July 2026


Finally, our model recovers turbulent eddy diffusivity as the integral of the curve in Fig. 1, $K_\theta = \int_0^\infty \mathrm{d}k\,\mathrm{E}_{\mathrm{w}\theta} G^{-1}$, after which the molecular baseline $\nu/\mathrm{Pr}$ is added to obtain total diffusivity.

### 2.4 Parameter values

#### 2.4.1 Proportionality constant $\mathbf{C}_{\mathbf{w}\boldsymbol{\theta}}$

$\mathrm{C}_{\mathrm{w}\theta}$ has been determined from DNS to be roughly 1.5 for high Reynolds numbers (Watanabe and Gotoh, 2007). Note that O'Gorman and Pullin (2005) arrived at the same functional form as the Lumley scaling by analytic means, albeit with a much larger $\mathrm{C}_{\mathrm{w}\theta} \approx 3.5$, which would entail $\tilde{K}_\theta$ 2-3 times as large. As we show in Appendix B, one can also deduce $\mathrm{C}_{\mathrm{w}\theta} \approx 0.95$ from Lagrangian decorrelation times by comparing Eq. 9 with Eq. B4. For low to intermediate Reynolds numbers, Watanabe and Gotoh (2007) proposed a Reynolds number dependent scaling $\mathrm{C}_{\mathrm{w}\theta} \propto \mathrm{Re}^{0.5-\delta/2}$ with $\delta = 0.78$ for $\mathrm{Re} < \mathcal{O}\left(10^6\right)$, $\mathrm{C}_{\mathrm{w}\theta}(\mathrm{Re} \geq 10^6) = 1.5$. This scaling conveniently fixes both $\mathrm{C}_{\mathrm{w}\theta}$ and $s_c = -7/3$ (see below) in a consistent manner; we will therefore prefer this scaling for computations.

#### 2.4.2 Spectral slope of the large scale $s_a$

Based on the calculations in Appendix A, $s_a$ is not very important (see Eq. A2). Reasonable values are between 2 and 4 (Chasnov, 1994), supported by the cospectrum inequality of O'Gorman and Pullin (2005).

#### 2.4.3 Spectral slope of the stratified range $s_b$

The large-scale anisotropy of stratified turbulence complicates computation of cospectra. In particular, while it is often assumed that scales larger than $\ell_O$ do not contribute to vertical flux of scalars, evidence is ambiguous on how the scalar flux is distributed in the wavenumber band between $\ell_O$ and $\ell_h$ (Riley and Lindborg, 2012). The main point of contention is whether $F_\theta$ receives its main contributions from the wavenumbers around $1/\ell$ or those around $1/\ell_O$. Accordingly, many different spectral forms have been proposed for $\tilde{K}_\theta$ and $\mathrm{E}_{\mathrm{w}\theta}$ in the wavenumber range $k < 1/\ell_O$, based on a variety of scaling arguments. Hence, there are widely diverging hypotheses for the value of $s_b$ in the literature, ranging from $1/3$ to less than $-1$ (Riley and Lindborg, 2012). Holloway (1986) proposed a form that amounts to $\mathrm{E}_{\mathrm{w}\theta} \sim k^{1/3}$ for $k \ll 1/\ell_O$.

The *additional* contribution to $\tilde{K}_\theta$ from the $\mathrm{Fr}_h < 1$ range (on top of the value at $\mathrm{Fr}_h = 1$ from Eqs. 9 or B4) is

$$\tilde{K}_\theta^{\mathrm{strat}} \sim \int_{1/\ell_h}^{1/\ell_O} \mathrm{d}k\,k^{s_b} \sim \begin{cases} 1 - \mathrm{Fr}_h^{3(s_b+1)/2} & s_b \neq -1 \\ \log\left(\mathrm{Fr}_h^{-3/2}\right) & s_b = -1, \text{ not normalized} \end{cases} \tag{10}$$

where the constant of proportionality needs to be chosen from continuity of $\mathrm{E}_{\mathrm{w}\theta}$ at $k = 1/\ell_O$. Hence, if the spectral exponent $s_b$ in $\mathrm{E}_{\mathrm{w}\theta} \sim k^{s_b}$ is larger than $-1$, mixing happens mostly at the Ozmidov scale, whereas in the opposite case, scalar mixing happens predominantly at the integral length scale.

The main consequence of $s_b < -1$ is an increasing $\tilde{K}_\theta$ with decreasing $\mathrm{Fr}_h$ for $\mathrm{Fr}_h < 1$ (Fig. 2A). Riley and Lindborg (2012) proposed $\mathrm{E}_{\mathrm{w}\theta} \sim k_h^{-1}$ and addressed the resulting logarithmic divergence of $\tilde{K}_\theta$ at low $\mathrm{Fr}_h$ by introducing an ad-hoc

https://doi.org/10.5194/egusphere-2026-4080
Preprint. Discussion started: 21 July 2026


scaling $\mathrm{E}_{\mathrm{w}\theta} \sim k_h^{-1} \log(\ell_h/\ell_O)$, which essentially forces a constant $\tilde{K}_\theta$ at $\mathrm{Fr}_h \leq 1$ and the buoyancy flux to be of order $\epsilon$. As we will see, based on observed $\tilde{K}_\theta$-$\mathrm{Fr}_h$ scalings alone (see Sec. 4), it is not possible to decide between a power law with a high exponent (which forces mixing to happen predominantly at $\ell_O$) and such an ad-hoc logarithmic scaling.

Above, we already addressed the fact that $s_b$ is only the integrated result of potentially very different spectral slopes in the vertical and horizontal directions. Much more tenuous, at this point, is the assumption that we can use parameters largely derived from unstratified turbulence, especially $\mathrm{C}_{\mathrm{w}\theta}$ and $s_c$, even when there is a large wavenumber band of stratified turbulence. Again, the justification for this procedure will lie in its success at describing field and DNS observations.

#### 2.4.4 Spectral slope in the inertial-convective range $s_c$

The classical Lumley $\mathrm{E}_{\mathrm{w}\theta} \sim k^{-7/3}$ scaling (Eq. 7) for fully developed turbulence has been criticised, with theoretical bounds on the exponent $s_c$ from $-7/3$ to $-5/3$ (Bos et al., 2004). Further, $-7/3$ is sometimes not observed in nature or numerical experiments. The approach to asymptotic conditions may simply be too slow (Gotoh and Yeung, 2012). Mydlarski and Warhaft (1998) and Mydlarski (2003) observed $\mathrm{E}_{\mathrm{w}\theta} \sim k^{-5/3}$ in wind tunnel turbulence, with a very slow approach towards $\sim k^{-7/3}$. Bos et al. (2005) suggested that realizing the $\sim k^{-7/3}$ scaling may require $\mathrm{Re} \gtrsim 10^7$. Also note that the $-5/3$ slope naturally emerges as the maximum permitted by the cospectrum inequality by O'Gorman and Pullin (2005), see Eq. A1. Even so, in the ocean, observations by and large have confirmed the -7/3 scaling (Pond et al., 1971; Kaimal, 1973). Gargett and Moum (1995) observed a rather narrow inertial-convective range with somewhat uncertain values between -5/3 and -7/3, while other measurements were inconclusive (Lienhard V and Van Atta, 1990; Moum, 1996).

This means the present model may need to account for finite Reynolds numbers. For isotropic turbulence, Watanabe and Gotoh (2007) solved the same problem in a different way: They found that the exponent $s_c$ was in fact close to $-7/3$ even for low Reynolds numbers. Rather, they constructed a full scaling for $\mathrm{C}_{\mathrm{w}\theta}$ dependent on Re (see above). In the following, we will use this scaling as it allows a precise definition of Reynolds number dependence.

#### 2.4.5 Spectral rolloff in the viscous subrange, $\beta$

We take $\beta = 6.7$ (Khurshid et al., 2018). As the viscous-convective and viscous-diffusive subranges see a rapid rolloff (O'Gorman and Pullin, 2005), calculated $\tilde{K}_\theta$ does not strongly depend on this value.

#### 2.4.6 Examples and variability

Some example spectra are shown in Fig. 1. Resulting $\tilde{K}_\theta$ estimates show considerable dependency of $\tilde{K}_\theta$ on $s_b$ for $\mathrm{Fr}_h$<1 (Fig. 2A), corresponding to the importance of the contribution of the stratified wavenumber band to buoyancy transport (Riley and Lindborg, 2012). Low values of $\mathrm{Re}_\mathrm{b}$ also impact $\tilde{K}_\theta$ (Fig. 2B), corresponding to the decrease in mixing efficiency at low $\mathrm{Re}_\mathrm{b}$. Smoothing ($\varphi$) only slightly decreases $\tilde{K}_\theta$ (Fig. 2C), in particular around $\mathrm{Fr}_h = 1$.

https://doi.org/10.5194/egusphere-2026-4080
Preprint. Discussion started: 21 July 2026


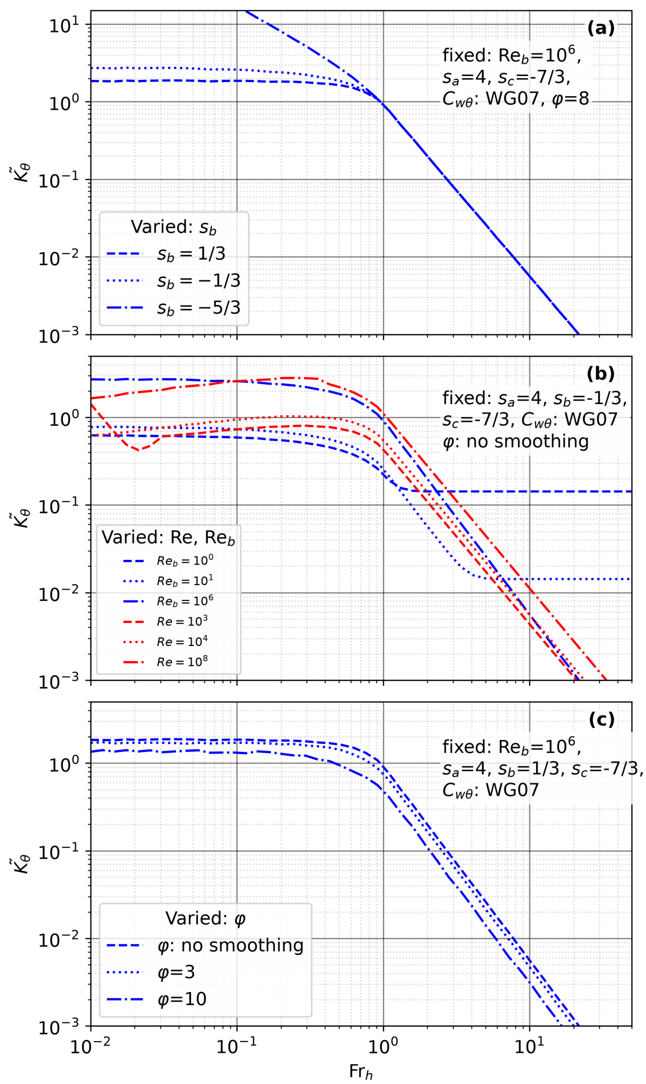


**Figure 2.** $\tilde{K}_\theta$ as a function of $\mathrm{Fr}_h$ for various combinations of $s_b$, Re, $\mathrm{Re_b}$, and $\varphi$ (see text). "WG07" refers to the $\mathrm{C}_{w\theta}$ scaling proposed by Watanabe and Gotoh (2007). Panel A: $\mathrm{Re_b} = 10^6$, $\varphi = 8$. Panel B: $s_b = -1/3$, $\varphi = 1$. Panel C: $s_b = 1/3$, $\mathrm{Re_b} = 10^6$. Note that $\mathrm{Re} \equiv \mathrm{Fr}_h^{-2}\mathrm{Re_b}$ by definition.

https://doi.org/10.5194/egusphere-2026-4080
Preprint. Discussion started: 21 July 2026


### 2.5 One-dimensional and three-dimensional spectra

Finally, we calculate the one-dimensional transverse cospectrum $\mathrm{E}^{1T}_{\mathrm{w}\theta}$ from the three-dimensional shell-summed cospectrum $\mathrm{E}_{\mathrm{w}\theta}$. This will be necessary to compare our model to eddy covariance observations (see Sec. 3). The one-dimensional transverse cospectrum is (O'Gorman and Pullin, 2003; Watanabe and Gotoh, 2007)

$$\mathrm{E}^{1T}_{\mathrm{w}\theta}(k) = -\frac{k^2}{2}\frac{\mathrm{d}}{\mathrm{d}k}\frac{\mathrm{E}^{1L}_{\mathrm{w}\theta}(k)}{k} \tag{11}$$

with the one-dimensional longitudinal cospectrum

$$\mathrm{E}^{1L}_{\mathrm{w}\theta}(k) = \frac{3}{4}\int_k^\infty \mathrm{d}k' \frac{k'^2 - k^2}{k^3}\mathrm{E}_{\mathrm{w}\theta}(k'). \tag{12}$$

Examples are shown in Fig. 3. Note that both of these expressions for $\mathrm{E}^{1L}_{\mathrm{w}\theta}$ and $\mathrm{E}^{1T}_{\mathrm{w}\theta}$ assume isotropy, which is violated below $1/\ell_O$, although it is unknown to which extent.

### 2.6 Monin-Obukhov similarity scaling

Lastly, in relation to the boundary layer measurements we will use to evaluate the model spectrum, we also quickly explore Monin-Obukhov similarity (Obukhov, 1971), which has been found to describe the effects of stratification on vertical fluxes in the ice-ocean boundary layer reasonably well (McPhee, 2008). Briefly, vertical diffusivity at vertical distance $z$ from the interface is reduced by a stability factor $\phi(z/L) = 1 + \gamma z/L$ with an empirical constant $\gamma \approx 4\ldots 8$ and the Monin-Obukhov length $L = U^3/(\kappa F_b)$. (The stability factor $\phi$ is unrelated to the spectral smoothing factor $\varphi$ and only used in this section.) In the latter, $\kappa \approx 0.4$ is the von Kármán constant, i.e. $K_\rho \simeq U\ell/\phi$, and $U$ in this subsection specifically denotes a friction velocity. In the ocean, friction velocity has been shown to be tightly coupled to the root mean square turbulent velocity (McPhee, 2008). Inserting the latter expression for $K_\rho$ into $\tilde{K}_\rho = K_\rho N^2/\epsilon$ and assuming Taylor scaling $\epsilon = U^3/\ell$ produces

$$\tilde{K}_\rho = (\mathrm{Fr}_h^2 \phi)^{-1}. \tag{13}$$

Assuming that $z$ is small enough that the governing lengthscale is $\ell = \kappa z$ (which typically is the case in the uppermost few meters, see McPhee, 2008) and again assuming Taylor scaling, then $z/L = \kappa z F_b/U^3 = F_b/\epsilon = \tilde{K}_\rho$. Inserting the definition of the stability factor $\phi$ and $F_b = K_\rho N^2$ in Eq. 13 yields a quadratic equation for $\tilde{K}_\theta$, and in consequence

$$\tilde{K}_\rho \sim \frac{\sqrt{1 + 4\gamma/\mathrm{Fr}_h^2} - 1}{2\gamma}, \tag{14}$$

up to order one constants. Note that this resembles the intermediary $\Gamma \sim \mathrm{Fr}_h^{-1}$ and unstratified $\Gamma \sim \mathrm{Fr}_h^{-2}$ scaling regimes of Garanaik and Venayagamoorthy (2019) and Mashayek et al. (2021).

## 3 Field and numerical observations

This study uses data from a combination of field studies (eddy covariance, free-falling profilers) and Direct Numerical Simulation (DNS). Table 1 summarizes the data sources used in this study.

https://doi.org/10.5194/egusphere-2026-4080
Preprint. Discussion started: 21 July 2026


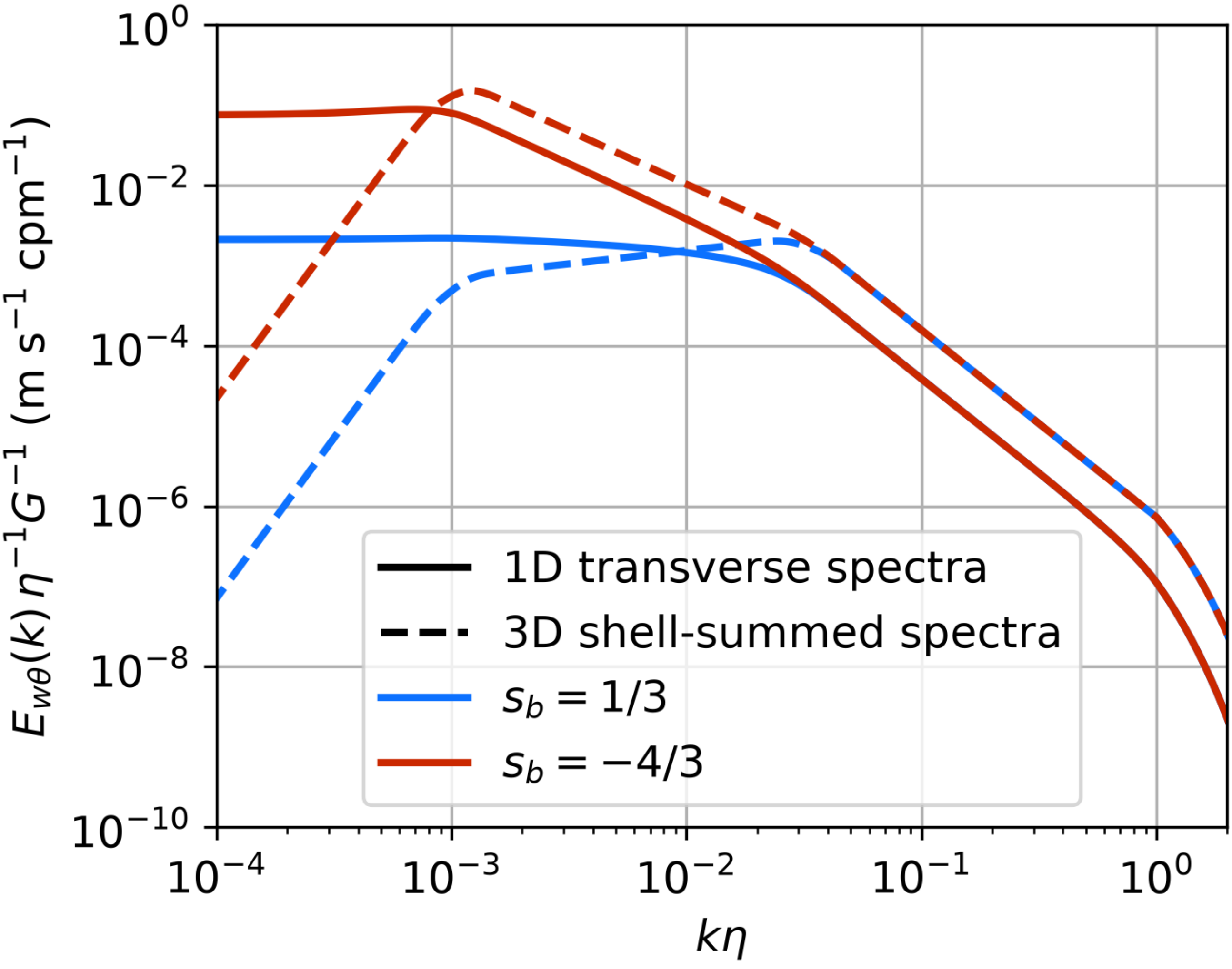


**Figure 3.** Example model spectra of $\mathrm{E}_{\mathrm{w}\theta}$ (dashed lines) and $\mathrm{E}^{1T}_{\mathrm{w}\theta}$ (solid lines) for $s_b = 1/3$ (blue) and $s_b = -4/3$ (red). The remaining parameters are $s_a = 4$, $s_c = -7/3$, $\varphi = 2$, $\mathrm{Fr}_h = 0.1$, and $\mathrm{Re}_\mathrm{b} = 1000$.

https://doi.org/10.5194/egusphere-2026-4080
Preprint. Discussion started: 21 July 2026


### 3.1 Direct Numerical Simulation (DNS)

Multiple studies have presented DNS of stratified turbulence and reported $\Gamma$ as a function of $\mathrm{Fr}_h$ and $\mathrm{Re_b}$. We will compare our model (see previous section) to DNS of Kelvin-Helmholtz billows of Smyth et al. (2001) (abbreviated SMC01), the sheared DNS of Shih et al. (2005) (abbreviated SKIF05), the forced DNS of Maffioli et al. (2016) (abbreviated MBL16) and the decaying DNS of Garanaik and Venayagamoorthy (2019) (abbreviated GV19). See Table 1 for each data set's definition of $\Gamma$.

### 3.2 Oceanic microstructure observations

Many studies have reported mixing efficiencies from oceanic microstructure, but only few that we are aware of also reported dependency on both $\mathrm{Re_b}$ and any variant of the Ozmidov-Thorpe/Ellison length scale ratio, e.g. $R_{OT} \equiv \ell_O/\ell_T \approx \ell_O/\ell_E$ and variations thereof (Dillon, 1982; Smyth et al., 2001; Ijichi and Hibiya, 2018). Briefly, the Thorpe length scale $\ell_T$ is the root mean square vertical displacement of a water parcel compared to a hypothetical density reordering to achieve a stable water column; in essence, it measures the size of density overturns (Thorpe, 1977). The Ellison length scale $\ell_E$ is closely related, being the root mean square deviation of the temperature compared to the background temperature gradient over a turbulent patch. In the following, we will assume $\ell_T \simeq \ell_E$; e.g., Smyth et al. (2001) discuss the issue in more detail.

To convert between $R_{OT}$ and $\mathrm{Fr}_h$, we use the scaling relation displayed in Fig. 3 of Garanaik and Venayagamoorthy (2019), but note that this scaling is derived from DNS data alone and may require revision if oceanic data are shown to be very different.

In such microstructure measurements, $\Gamma$ is usually estimated using the Osborn-Cox relation (Osborn and Cox, 1972), which crucially assumes isotropy, stationarity and negligible transport terms. From it and Eq. 2, Oakey (1982) derived

$$\Gamma_\chi \approx \frac{\epsilon_\theta N^2}{G^2 \epsilon}, \tag{15}$$

where $\epsilon_\theta$ is the scalar variance dissipation. Eq. 15 is usually taken to yield a useful estimate of $\Gamma$ even though the underlying assumptions are rarely fulfilled in the ocean (Smyth et al., 2001). For the lack of adequate observations of density and/or salinity microstructure, one often resorts to using temperature, further assuming $K_T = K_\rho$, recovering the definition of $\Gamma_\chi$ of Caulfield (2020).

### 3.3 Eddy covariance in the ice-ocean boundary layer

Turbulent fluxes estimated through eddy covariance are the closest to the actual definition of $F_\theta$ as a covariance of turbulent fluctuations. Unfortunately, the eddy covariance technique needs a stable platform, which in the ocean interior is a challenge. However, such a platform is readily available in the ice-ocean boundary layer (IOBL), where turbulent fluxes have been regularly measured for decades (McPhee, 2008).

We here build upon a time series of approx. 6000 15-minute segments of temperature and three-dimensional velocity sampled at 2 Hz, 1 m under drifting sea ice in the Arctic Ocean from March to June 2015 (Peterson et al., 2017), in the following abbreviated as PFMR17. Briefly, data were analyzed in 15-minute segments, for each of which current velocity was rotated into an along-current reference frame and stationarity was tested as well as absence of contamination of fluxes from swell.

https://doi.org/10.5194/egusphere-2026-4080
Preprint. Discussion started: 21 July 2026


**Table 1.** Data sources for the present study: reference, abbreviation used in text and Fig. 4, Prandtl number Pr, and definition of $\Gamma$ employed. Also note the description of data extraction in Appendix D. [a]$\mathrm{Pr} = 4$ case omitted in the present study. [b]$\Gamma_\chi$ values as computed by Garanaik and Venayagamoorthy (2019). [c]Estimates use ocean temperature microstructure. [d]represents thermally stratified air, not the ocean. However, this Prandtl number is still sufficiently high to not cause large corrections, as was verified by generating the SKIF05 curve in Fig. 5 with both Pr=1 and Pr=0.72 (comparison not shown).

| Reference | Abbreviation | Source | Forcing | Pr | $\tilde{K}_\theta$, $\Gamma$ definition |
|---|---|---|---|---|---|
| This study | model | — | — | variable | $\tilde{K}_\theta$ |
| Smyth et al. (2001) | SMC01 | DNS | KH billow | 1, 7 [a] | $\Gamma_\mathcal{M}$ |
| Shih et al. (2005) | SKIF05 | DNS | sheared | 0.72 [d] | $\Gamma_\chi$ [b] |
| Maffioli et al. (2016) | MBL16 | DNS | forced | 1 | $\Gamma_\chi$ |
| Garanaik and Venayagamoorthy (2019) | GV19 | DNS | decaying | 1 | $\Gamma_\chi$ |
| Smyth et al. (2001) | SMC01 | ocean, microstructure | ocean interior | — | $\Gamma_\chi$ [c] |
| Ijichi and Hibiya (2018) | IH18 | ocean, microstructure | ocean interior | — | $\Gamma_\chi$ [c] |
| reanalysis of Peterson et al. (2017) | PFMR17 | ocean, eddy covariance | boundary layer | — | $\Gamma$ |

Temperature and velocity components were detrended before calculating auto- and co-spectra. We estimated $\epsilon$ from the inertial subrange of each smoothed 15-minute autospectrum of vertical velocity and $\mathrm{K} = (u^2 + v^2 + w^2)/2$ with the three velocity components $u$, $v$, $w$. For details, the reader is referred to Peterson et al. (2017). Vertical temperature gradient $G$ and buoyancy frequency $N^2$ were estimated as regressions of temperature and density over 1 to 3 dbar from nearby drops of a high-resolution microstructure profiler (Meyer et al., 2017). In cold water, salinity determines buoyancy. However, measuring turbulent salinity fluctuations is far more challenging than those of temperature (Nash and Moum, 1999). We therefore determined $F_b$ from the upward heat flux $F_T$ assuming all of it goes towards melting the ice, i.e. no heat or salt fluxes through the sea ice itself (McPhee, 2008). Concretely, salt flux $F_S = F_T(S_0 - S_\text{ice})/Q_L$ with $Q_L = 73.3\,\mathrm{K}$ the latent heat for melting sea ice divided by specific heat of sea water, interface salinity $S_0$ approximated as mean salinity measured at 1 m below the ice, $S_\text{ice} = 4$, and buoyancy flux $F_b = g(\beta_S F_S - \alpha_T F_T)$ with gravitational constant $g = 9.81\,m\,s^{-2}$ and saline contraction and thermal expansion coefficients $\beta_S$ and $\alpha_T$.

Finally, we calculated $\Gamma = F_b/\epsilon$, $\mathrm{Fr}_h = U/(N\ell)$, and $\mathrm{Re_b} = \epsilon/(\nu N^2)$. For $U$, we used the ice-ocean interface friction velocity. For $\ell$, we used $\kappa z = 0.4\ m$ for the distance $z$ below the ice-ocean interface, which was consistent with observed but very noisy estimates of mixing length. Note that since stationarity is ensured for each of the segments, $\Gamma$ derived in this way makes a much stronger constraint on the irreversible mixing. After tests for stationarity and excluding segments unsuitable for our analysis ($G < 0\,K\,m^{-1}$, $N^2 < 10^{-5}\mathrm{s}^{-2}$, $\langle w'T' \rangle < 0\,K\,m\,s^{-1}$) or excluding parameter ranges with too few data points to calculate reliable average $\tilde{K}_\theta$ ($\mathrm{Fr}_h < 0.5$, $\mathrm{Re_b} < 50$), approx. 300 segments remained for final analysis. ($'$ denotes the residual, turbulent quantity after subtracting the segment average $\langle\cdot\rangle$.)

https://doi.org/10.5194/egusphere-2026-4080
Preprint. Discussion started: 21 July 2026


## 4 Results and Discussion

This section evaluates the present model of $\tilde{K}_\theta$ against observations. By practical necessity, we compare it to published estimates of $\Gamma$, and accordingly make all the necessary assumptions as detailed above.

### 4.1 Comparison with observational data

Our model and all available data agree on the $\Gamma \sim \mathrm{Fr}_h^{-2}$ scaling for $\mathrm{Fr}_h > 1$ (Fig. 4). It also compares favourably with existing DNS (Smyth et al., 2001; Shih et al., 2005; Maffioli et al., 2016; Garanaik and Venayagamoorthy, 2019) for $s_b \approx 1/3$ (Fig. 4), in particular the flattening out of $\tilde{K}_\theta$ for $\mathrm{Fr}_h \lesssim 1$. We therefore use the 1/3 spectrum (Holloway, 1986) as a model type for the DNS data throughout the paper. This is to be understood as an illustration, not as an endorsement based on a statistical analysis.

However, ocean microstructure data from the ocean interior (Smyth et al., 2001; Ijichi and Hibiya, 2018) hint at a very different scaling of $\tilde{K}_\theta$ with $\mathrm{Fr}_h$ for $\mathrm{Fr}_h < 1$ (Fig. 4) than those from DNS. To reproduce with our model, they require $s_b \approx -4/3$, much closer to the spectral slope $s_c$ of $-7/3$ in the (presumably isotropic) inertial-convective subrange.

Modelled $\tilde{K}_\theta$ compares favourably with $\mathrm{Re_b}$ scalings reported in the literature and from eddy covariance in the ice-ocean boundary layer (Fig. 5). In particular, it improves on a previous $\Gamma = \Gamma(\mathrm{Re_b})$ regression (Bouffard and Boegman, 2013) and achieves excellent agreement with DNS even where $\mathrm{Fr}_h$, and hence $\tilde{K}_\theta$, values differ between different DNS experiments (compare MBL16, PFMR17, and GV19). Deviations in the sheared DNS (SKIF05, Shih et al., 2005) may be due to deviations in $\mathrm{Fr}_h$ as well as their using $\mathrm{Pr} = 0.72 < 1$ for temperature-stratified air, not water. However, the latter can not be the sole explanation because the inclusion of such a narrow inertial-diffusive wavenumber range ($1/\eta_B < k < 1/\eta$) in the model would only slightly lower resulting $\tilde{K}_\theta$ (not shown). Like others before us, we conclude that $\mathrm{Re_b}$ may be useful (Bouffard and Boegman, 2013; Mashayek et al., 2017) but ultimately not sufficient as a single parameter for parameterizing $\tilde{K}_\theta$ or $\Gamma$ in the ocean (Mater and Venayagamoorthy, 2014; Scotti and White, 2016; Monismith et al., 2018).

### 4.2 Disagreement between DNS and ocean observations for low $\mathrm{Fr}_h$

Our model can only reproduce the scaling measured in the ocean when we suppose a spectral slope for stratified scales of $s_b \approx -4/3$, markedly different from the slightly positive value deduced for the DNS data ($s_b \approx 1/3$ works, but is inspired by Holloway (1986); similar values work equally well). Neither the eddy covariance data from the sea-ice ocean boundary layer (Peterson et al., 2017) nor the Kelvin-Helmholtz billow DNS of Smyth et al. (2001) with $\mathrm{Pr} = 7$ reach low enough $\mathrm{Fr}_h$ to confidently distinguish between the two. In fact, the latter's DNS with $\mathrm{Pr} = 1$ interestingly fall right between the other DNS and the ocean observations. Smyth et al. (2001) speculated that it might be due to the tendency of Eq. 15 to overestimate $\Gamma$ in young turbulence caused by breakdown of the Osborn-Cox assumptions, notably isotropy (also shown by Garanaik and Venayagamoorthy (2018); Klema and Venayagamoorthy (2023)), and of the validity of using the mean temperature gradient. The departure from isotropy for instance may overestimate $\epsilon_b$ and hence $\Gamma_\chi$ by as much as a factor of 2 (Garanaik and Venayagamoorthy, 2018). Comparing eddy diffusivities derived from ocean microstructure using the Osborn-Cox method with those derived from a model fit to $R_{OT}$, the findings of Smyth et al. (2001) seem consistent with a similar factor 2 uncertainty

https://doi.org/10.5194/egusphere-2026-4080
Preprint. Discussion started: 21 July 2026


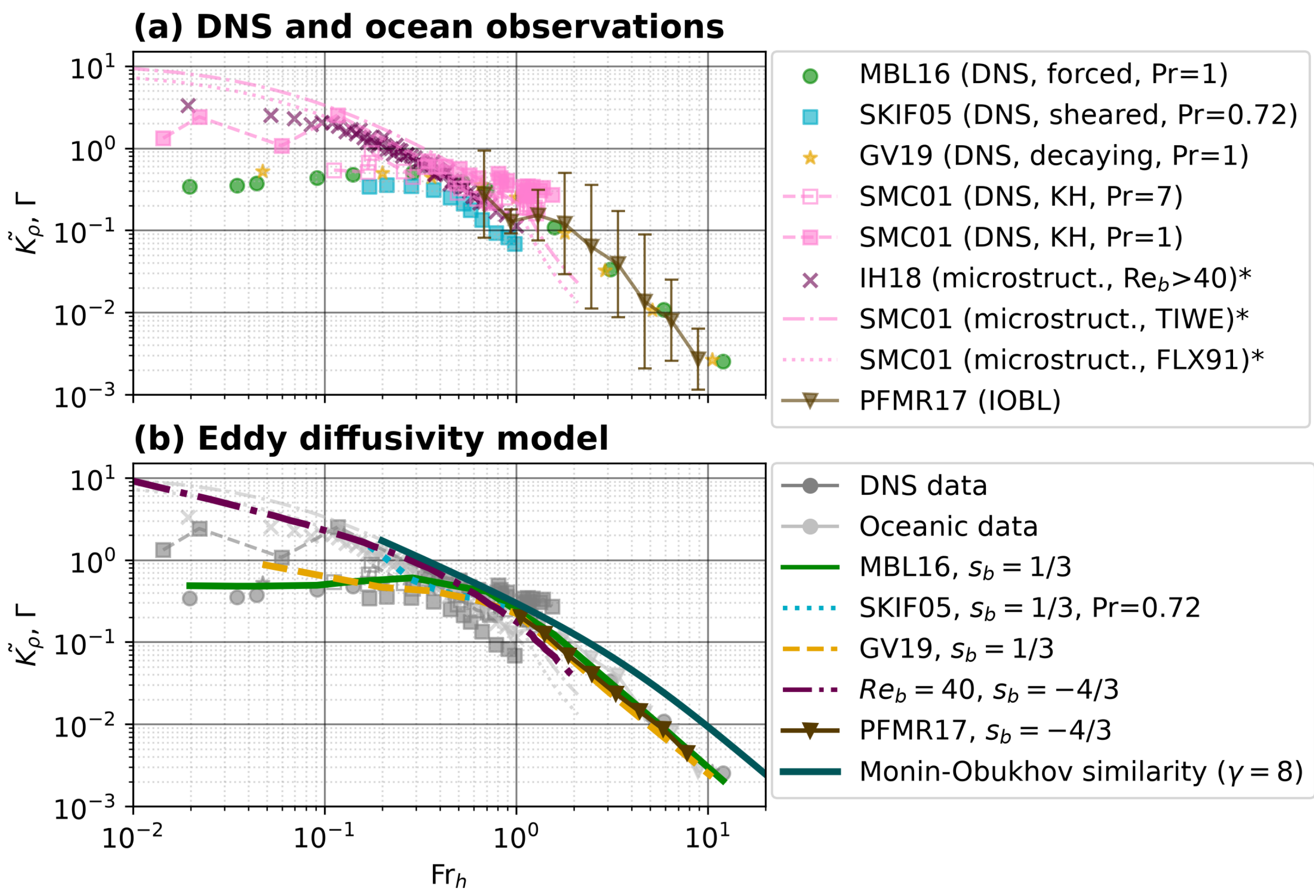


**Figure 4.** $\tilde{K}_\rho$ and $\Gamma$ as a function of horizontal Froude number $\mathrm{Fr}_h$. See Table 1 and Appendix D for data sources. SMC01 (TIWE, FLX91) refer to two different field experiments as described by Smyth et al. (2001). (A): For data sources, see Tab. 1 and Appendix D. * IH18 and SMC01 were transformed from the Ozmidov-Thorpe/Ellison scale ratios using Fig. 3 of Garanaik and Venayagamoorthy (2019) and assuming that $\ell_T \simeq \ell_E$. (B): Predictions using our $\mathrm{E}_{w\theta}$ model spectrum as well as Monin-Obukhov similarity.

https://doi.org/10.5194/egusphere-2026-4080
Preprint. Discussion started: 21 July 2026


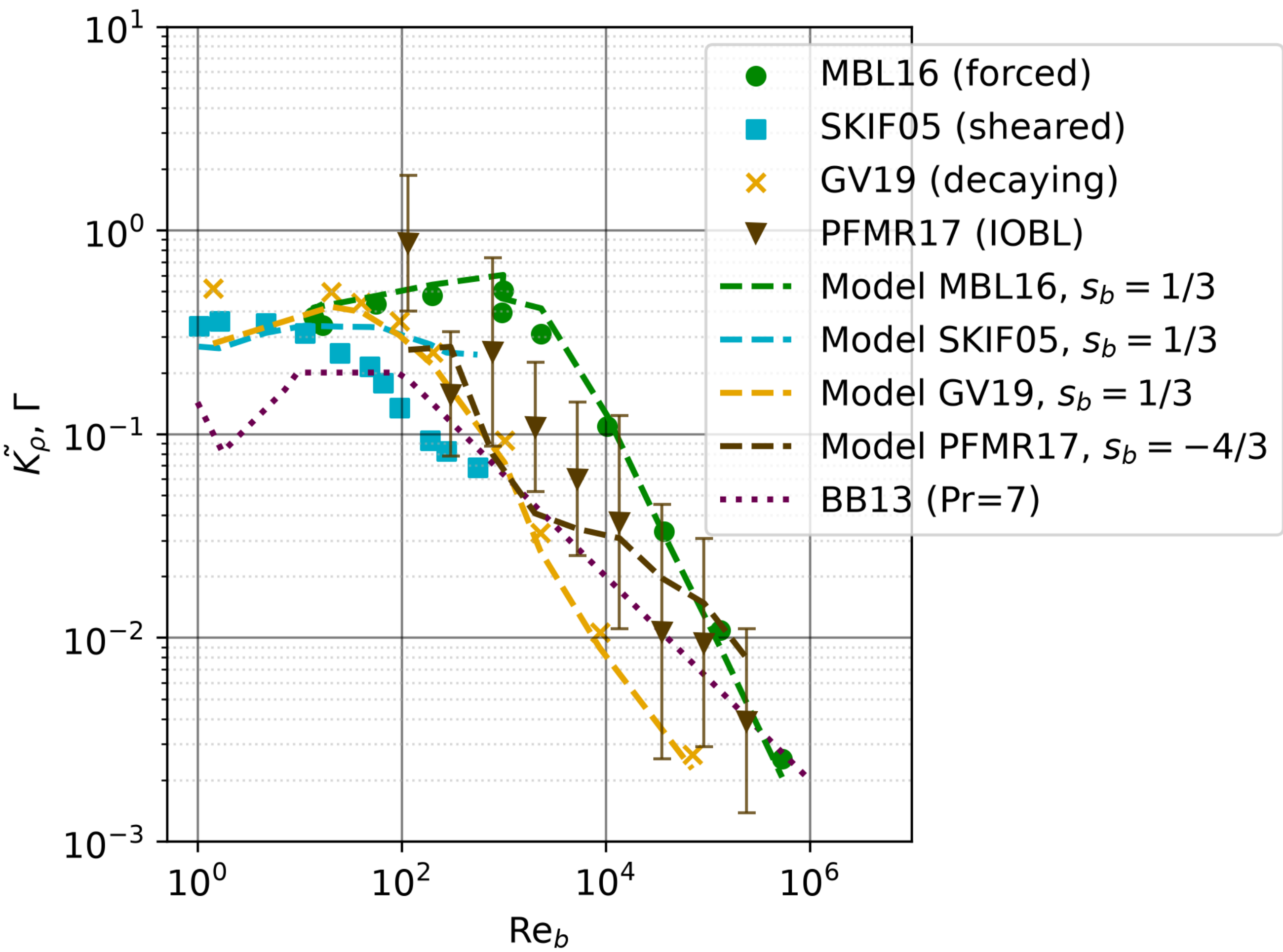


**Figure 5.** $\tilde{K}_\rho$ and $\Gamma$ as function of $\mathrm{Re_b}$. For data sources, see Tab. 1 and Appendix D. The dotted line (BB13) shows a regression based on oceanic and DNS observations (Bouffard and Boegman, 2013).

in the Osborn-Cox assumption (see their Fig. 17). This line of thought would then close part but not all of the gap between the DNS of Kelvin-Helmholtz billows and the ocean observations (significantly larger than the factor 2 just mentioned).

To reconcile the difference between the remaining DNS and ocean microstructure observations for $\mathrm{Fr}_h \ll 1$ (and since Pr does not exert such a strong influence over $\tilde{K}_\theta$), a possible remaining explanation is that turbulence generation and/or mixing processes work differently in the ocean than in those DNS setups. This may be a consequence of shear, strain, or turbulence in the oceanic background, as well as the generation mechanism. The latter factor may be especially important if we accept that Kelvin-Helmholtz instabilities are what is underlying much of oceanic turbulence and in light of the closer agreement between the DNS thereof and oceanic observations. In other words, the difference between ocean observations and the DNS of Kelvin-Helmholtz billows at $\mathrm{Pr} = 1$ on the one hand, and the remaining DNS on the other hand, may be a result primarily of forcing. Indeed, Maffioli et al. (2016) maintained stationary turbulence using a decorrelated-in-time Gaussian body force and Garanaik and Venayagamoorthy (2019) "initialized [the flow] with a Gaussian isotropic three-dimensional solenoidal velocity field and allowed to evolve and decay under the influence of a constant background stratification", neither of them reproducing a collapsing Kelvin-Helmholtz billow.

There are two additional strong arguments supporting that line of thought: First, Monin-Obukhov similarity, which gives a well-tested empirical scaling of turbulent transfer in boundary layers, indicates that the intermediate $\Gamma \sim \mathrm{Fr}^{-1}$ range also deduced by Garanaik and Venayagamoorthy (2019), and, based on quite different reasoning, by Mashayek et al. (2021), might extend to lower $\mathrm{Fr}_h$ than the DNS results showed. Secondly, other DNS (for which $\Gamma$ was not directly reported) indicated that potential energy grew to approximately the same order of magnitude as kinetic energy (Riley and deBruynKops, 2003; Brethouwer et al., 2007), which has been interpreted to mean that the buoyancy flux, and hence $\Gamma$, would receive most of its contributions from scales around $\ell_h$, not $\ell_O$ (Riley and Lindborg, 2012). This, in turn, would imply that $\Gamma$ would continue increasing with smaller $\mathrm{Fr}_h$, in agreement with the oceanic observations (Fig. 4A).

Scalar-velocity cospectra then offer a tempting hypothesis: That the main discrepancy at $\mathrm{Fr}_h < \mathcal{O}(1)$ is a result of the spectral slope $s_b$ in the stratified range, which itself would be a result of the scales stirring the fluid. If turbulence is generated at scales $\ell_h \gg \ell_O$, $s_b$ would be smaller, whereas for forcing at scales closer to $\ell_O$, the spectral slope would naturally be flatter, the consequences of this being visible in Fig. 4B.

One also has to keep in mind that in order to pass between $\mathrm{Fr}_h$ and Ozmidov-Thorpe/Ellison scale ratios, we used Fig. 3 of Garanaik and Venayagamoorthy (2019) (see Appendix D), which is based on the three DNS data sets (Shih et al., 2005; Maffioli et al., 2016; Garanaik and Venayagamoorthy, 2019) that do *not* agree with ocean measurements. This might eventually necessitate recomputation of the scaling between $\mathrm{Fr}_h$ and Ozmidov-Thorpe/Ellison scale ratios based on ocean measurements or DNS more representative of ocean mixing. However, changing the $\mathrm{Fr}_h \sim R_{OT}$ scaling will not change the fact that DNS, besides potentially the one by Smyth et al. (2001), seem to plateau (for $\mathrm{Fr}_h$<1) at lower $\Gamma$ than ocean observations.

### 4.3 Other discrepancies between oceanic observations and DNS

Some other minor discrepancies and uncertainties are $\mathcal{O}(1)$: First, in the sheared DNS of Shih et al. (2005), $\Gamma$ starts decreasing at about half the $\mathrm{Fr}_h$ than both our model and the other data sets. We note that if $\mathrm{Fr}_h$ were about twice the plotted value, there

https://doi.org/10.5194/egusphere-2026-4080
Preprint. Discussion started: 21 July 2026


would not be significant disagreement anymore. It is not obvious whether this is a result of the $\mathrm{Fr}_h$ calculation, $\mathcal{O}(1)$ factors (see below), other numerical details of the DNS itself, or of the turbulence forcing mechanism in that experiment.

Secondly, besides smoothing of spectral peaks (our $\varphi$ parameter), dimensionless constants and scaling laws are only defined up to $\mathcal{O}(1)$. For instance, in the literature, different definitions of Fr and $\mathrm{Re_b}$ are used, such as $\mathrm{Fr} \sim \frac{U}{N\ell_h} \sim \frac{\epsilon}{N\mathrm{K}}$. These are usually connected by the Taylor scaling $\epsilon \sim U^3/\ell_h$. The constant of proportionality in the Taylor scaling is rarely reported. Peters et al. (1995), based on the Thorpe scale instead of $\ell_h$, give the constant of proportionality as 4. Maffioli and Davidson (2016), in a DNS of decaying stratified turbulence, corroborate the robustness of the scaling as such but give the constant of proportionality as around 0.2. This constant of proportionality is otherwise rarely reported and we hence refrain from quantifying it. In fact, the present analysis relies on the Taylor scaling by necessity. Incorporating a constant of proportionality different from 1 in the present model would be straightforward.

Third, slightly different variations on the Ozmidov-Thorpe scale ratios are used in the literature, such as $\frac{\ell_O}{\ell_E^{3/4}\ell_T^{1/4}}$ (Smyth et al., 2001) and $\frac{\ell_O}{\ell_T}$ (Smyth et al., 2001; Ijichi and Hibiya, 2018; Garanaik and Venayagamoorthy, 2019), where the definition of $\ell_O$ again varies by whether it is calculated using a mean or more representative bulk vertical density gradient across each turbulent patch. While $\ell_T \simeq \ell_E$ is a reasonable (and here, necessary) assumption, it could introduce factors of around 2-3 according to Fig. 8 of Smyth et al. (2001), and hence change $\mathrm{Fr}_h$ by a factor of up to 2.

### 4.4 Measured temperature-velocity cospectra in oceanic boundary layers

The ice-ocean boundary layer data (PFMR17 in Fig. 4) permit explicit calculation of transverse cospectra $\mathrm{E}^{1T}_{\mathrm{w}\theta}$ (Fig. 6). It is the real part $\mathcal{R}(\mathrm{E}_{\mathrm{w}\theta})$ which integrates to the vertical scalar flux. The imaginary part (the quadrature spectrum) has been shown theoretically to vanish in isotropic turbulence with a mean scalar gradient (O'Gorman and Pullin, 2003). In this regard, the spectra are noisy even after extensive averaging as evidenced by the frequent deviations from this theoretical expectation, $\mathcal{R}(\mathrm{E}_{\mathrm{w}\theta}) = \|\mathrm{E}_{\mathrm{w}\theta}\|$.

Apart from the noise, agreement of observed with model spectra is excellent in the inertial-convective range, where we observed an extended $s_c = -7/3$ slope. The $s_b = -4/3$ slope in the stratified range could not be clearly discerned, presumably because $\mathrm{Fr}_h$ was still quite elevated ($\gg 0.1$), leading to a narrow stratified wavenumber band.

The large scales ($k < 0.3\,\mathrm{cpm}$), however, see more substantial disagreement. We expect this to be a mix between anisotropy (mostly due to strong shear) and, potentially, contamination by non-turbulent motions such as swell and internal waves. In fact, uncompensated $\mathrm{E}_{\mathrm{w}\theta}$ showed no difference, in amplitude or shape, with $\mathrm{Re_b}$ changes from 10 to $10^6$ (Fig. 6C), in line with much weaker dependency of $F_b$ on $\mathrm{Re_b}$ than $\epsilon$ on $\mathrm{Re_b}$. This remarkable feature demonstrates that heat fluxes in the stratified IOBL specifically may be governed by additional processes not captured in our model spectrum.

Even so, given the considerable statistical uncertainty, the resulting $\tilde{K}_\theta$ are consistent with the present model computed with $s_b = -4/3$ as well as reasonably close to the Monin-Obukhov estimate (Fig. 4) within given uncertainties.

https://doi.org/10.5194/egusphere-2026-4080
Preprint. Discussion started: 21 July 2026


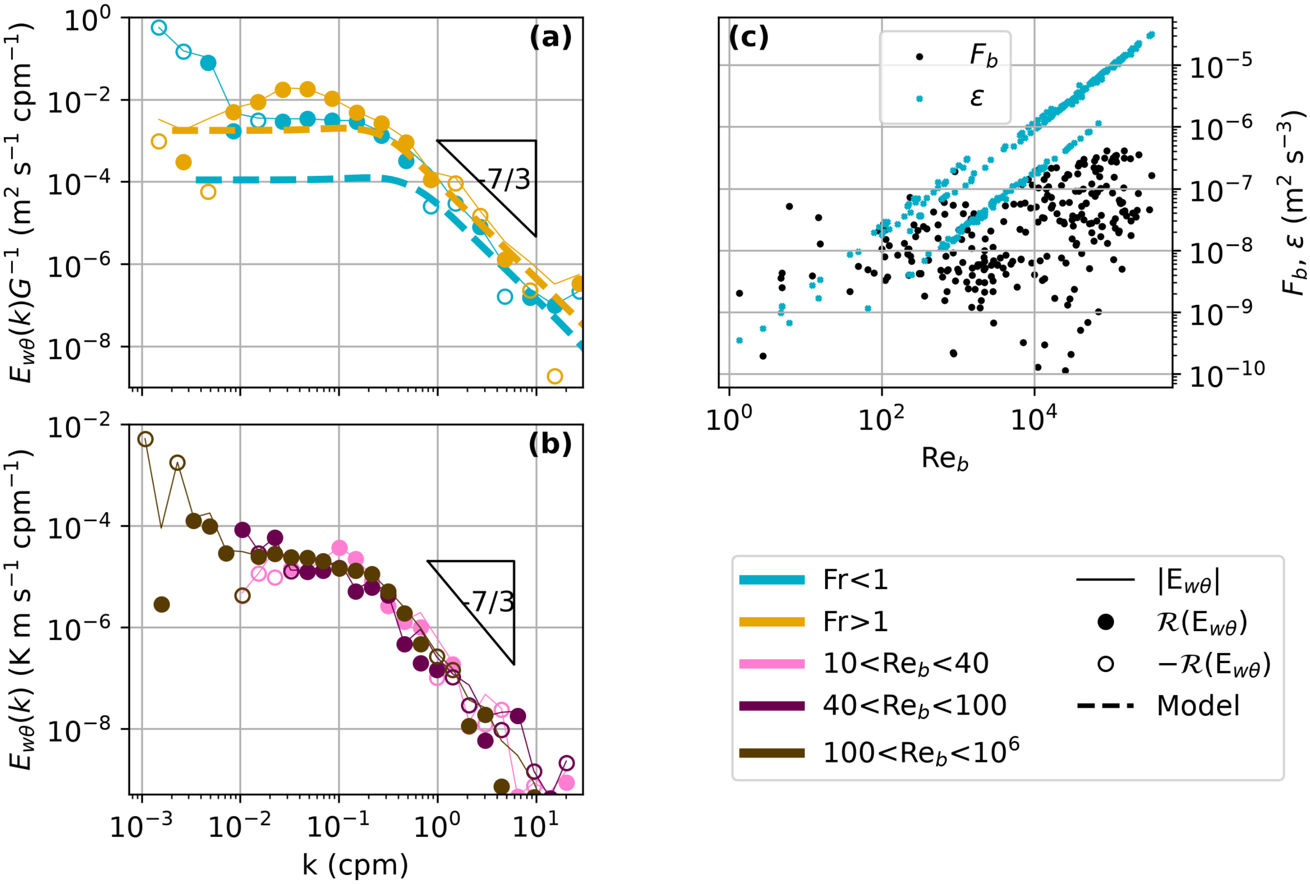


**Figure 6.** $E^{1T}_{w\theta}$ observed using eddy covariance in the ice-ocean boundary layer (entry PFMR17 in Fig. 4). A: Compensated $E^{1T}_{w\theta}(k)/G$, binned by Fr$_h$. Model spectra for $s_b = -4/3$, $s_c = -7/3$, $\varphi = 8$. B: $E^{1T}_{w\theta}(k)$ binned by Re$_b$. C: Buoyancy flux $F_b$ and dissipation as a function of Re$_b$. Note that in this plot, the few data points with Fr$_h$ < 0.5, Re$_b$ < 50 are included for illustrative purposes.

### 4.5 Summary and limitations

In summary, the present $\tilde{K}_\theta$ model unifies dependencies on both Re$_b$ and Fr$_h$. Even though extending the spectral shapes from isotropic, unstratified turbulence to stratified, low-Fr$_h$ turbulence required assuming that the inertial-convective subrange was not affected either in spectral slope or amplitude, $\tilde{K}_\theta$ overall compared favourably with observations, not only in scaling but also in absolute value. The Fr$_h < 1$ behaviour of $\tilde{K}_\theta$ differed between most existing DNS and observations of microstructure, which in our model we traced back to the spectral slope of E$_{w\theta}$ in the stratified wavenumber range.

Further limitations of our model that deserve attention in future work are:

https://doi.org/10.5194/egusphere-2026-4080
Preprint. Discussion started: 21 July 2026


1. Parameter choices for our model were guided by observations in turbulent flows. By design, this excludes the early, pre-turbulent stages of an instability (Smyth et al., 2001). Different parameters may be more appropriate for the pre-turbulent $\mathrm{E}_{\mathrm{w}\theta}$.

2. The Prandtl number enters our model through the width of the viscous-diffusive range, which rolls off exponentially and hence has a minor influence, as well as through the addition of a molecular diffusivity after the spectral integration. However, Salehipour and Peltier (2015) have shown that Pr itself may impact the evolution of secondary instabilities that in our model would only be felt indirectly presumably through modified spectral scaling parameters.

## 5 Conclusions and open questions

This study demonstrates the merits of using velocity-scalar cospectra, also called flux spectra, for parameterizing eddy diffusivity in the ocean. It proposes a spectral model which is by and large consistent with previously published DNS and ocean observations and provides a framework for understanding the observed differences between DNS and ocean microstructure. Notably, this paper unifies the simultaneous dependencies on $\mathrm{Fr}_h$ and $\mathrm{Re}_\mathrm{b}$, each of which has been studied in many previous publications. Note that we have refrained from an objective optimization analysis (such as a maximum likelihood estimate) to find optimal parameters for our model, as there are too many to comfortably settle their values with the currently available data. We consider this study first and foremost a proof of concept and an exploration of the parameter space.

To apply the present model for $K_\theta$, one needs measurements of the small scales (i.e., $\epsilon$, and hence $\mathrm{Re}_\mathrm{b}$) as well as the large scales of turbulence (i.e., $\ell$, $U$, or $K$, hence $\mathrm{Fr}_h$). Therefore, $\epsilon$ is not a comprehensive measure of "turbulent mixing". Instead, it becomes paramount to push development of techniques that can also determine $\mathrm{Fr}_h \sim U/(N\ell_h) \sim \epsilon/(N\mathrm{K})$. Mid-water-column measurements of $U$ or K are notoriously difficult, but techniques do exist (Peters et al., 1995). Findings in this study corroborate that ocean turbulence may be usefully described with the Ozmidov and Thorpe (or Ellison) length scale ratio $R_{OT}$ as a function of $\mathrm{Fr}_h$ (Mater et al., 2013; Garanaik and Venayagamoorthy, 2019). This provides a direct link from measurements of $\epsilon$, $N$, and $\ell_T$, all of which are usually accessible from vertical microstructure profiling, to eddy diffusivities.

The two most important parameters in our model are $\varphi$ and $s_b$. We treated $\varphi$ as an empirical parameter smoothing $\mathrm{E}_{\mathrm{w}\theta}$, but it is in principle fully quantifiable from measurements of $\mathrm{E}_{\mathrm{w}\theta}$. $\varphi$ acts to decrease the integrated value of $\mathrm{E}_{\mathrm{w}\theta}$, essentially reducing $\tilde{K}_\theta$ by an overall factor. $s_b$, the spectral slope in the stratified subrange between $1/\ell_h$ and $1/\ell_O$, governs behaviour at $\mathrm{Fr}_h \ll 1$. While scalar-velocity cospectra are reasonably well explored for a scalar mean gradient exposed to isotropic turbulence, modeling stratified eddy diffusivity required many assumptions. The overall agreement, not just in scaling, but even in absolute values, is all the more astonishing.

If oceanic values of $\Gamma$ are indeed strongly centered around 0.2 (Gregg et al., 2018) as evidenced by tracer release experiments (Ledwell et al., 1998, 2000), this in turn constrains the permissible Fr-Reb parameter space quite substantially. For $\mathrm{Re}_\mathrm{b} \gg 1$, we would then have to have $\mathrm{Fr}_h \simeq \mathcal{O}(1)$ and hence $\ell_h \simeq \ell_O$. This is consistent with the prevalence of $R_{OT} \simeq 1$ overturns in the ocean as noted by Mashayek et al. (2021).

https://doi.org/10.5194/egusphere-2026-4080
Preprint. Discussion started: 21 July 2026


The evolution of $\tilde{K}_\theta$ through the lifetime of a turbulent, decaying patch then directly falls back on the evolution of $\mathrm{Fr}_h$. In fact, the $\mathrm{Fr}_h = \mathrm{Fr}_h(R_{OT})$ relation (Garanaik and Venayagamoorthy, 2019) yields a difficult contradiction for the $\tilde{K}_\theta$ evolution that seems important to resolve in future work. On the one hand, the DNS of Smyth et al. (2001) demonstrated that $R_{OT}$ (hence $\mathrm{Fr}_h$ according to Garanaik and Venayagamoorthy (2019)) increased with time: $R_{OT} \sim \exp(t/3.2)$, where $t$ is measured in buoyancy periods. Indeed, small $R_{OT}$ is often used as an indicator of "young" turbulence (e.g., Mashayek et al., 2017; Ijichi and Hibiya, 2018). On the other hand, conservation arguments for the large scales of turbulence (Batchelor and Proudman, 1956; Saffman, 1967) predict decaying $\mathrm{Fr}_h$ (hence decaying $R_{OT}$). E.g., for decaying (isotropic) Batchelor turbulence ($\mathrm{E_u} \sim k^4$ for low $k$), one finds $U^2 \sim t^{-10/7}$ and $\ell \sim t^{2/7}$, hence $\mathrm{Fr} \sim t^{-1}$. Similar arguments can be made for stratified turbulence, and a similar scaling survives for $\mathrm{Fr}_h$ (Ch. 14.6, Davidson, 2013). Possible explanations for their diverging time evolution may relate to the fact that turbulence in the ocean is not homogeneous, but concentrated in patches that may obey different dynamics, or to influences from background shear and strain. Lastly, there is also the possibility that the relationship between $\mathrm{Fr}_h$ and $R_{OT}$ (equivalently, between $\ell_T$ and $\ell$) may not be as tight as supposed.

Based on the remaining inconsistencies between our model, DNS, and oceanic observations, we propose a few key uncertainties that may guide future research efforts: First, the evolution of length scales, $\mathrm{Fr}_h$, and $R_{OT}$ in a decaying patch of oceanic turbulence (see above). Second, the relation between $\mathrm{Fr}_h$ and $R_{OT}$. So far, it has been fixed based on DNS, but it should be tested in oceanic turbulence. Third, the reason for the divergence for $\mathrm{Fr}_h$<1 between Osborn-Cox estimates of $\tilde{K}_\theta$ (often the method of choice for oceanic microstructure observations) and those recovered from many DNS. Besides the nonstationarity and reversible contributions to mixing, it is unclear whether turbulence generation mechanisms or other processes occurring only in the ocean may play a role here. Internal waves, for instance, could change both the length scales at which oceanic turbulence is forced as well as the background strain and shear fields. This issue could in principle be tested using eddy covariance, but this would either have to be farther away from boundaries, or, in the case of under-ice boundary layers, with even faster sea ice melt to achieve lower $\mathrm{Fr}_h$.

Measurements of oceanic $\mathrm{E}_{\mathrm{w}\theta}$ spectra under varying conditions are also needed to refine the approach outlined in this paper. Aggregating $\mathrm{E}_{\mathrm{w}\theta}$ by $\mathrm{Fr}_h$ (or $R_{OT}$) may provide clues as to its time evolution and forcing scales. Note that for instance eddy covariance measurements of scalars and velocity even outside the oceanic boundary layer have previously been achieved (McPhee and Martinson, 1994), but our eddy covariance data set demonstrates that these need long timeseries before good statistics can be attained.

*Code and data availability.* We thank Andrea Maffioli for providing the forced DNS data (Maffioli et al., 2016). Ice-ocean boundary layer data were further processed from personal archives and those of Ilker Fer as well as from published datasets (Meyer et al., 2017; Peterson et al., 2017). Other data were visually scraped from the published graphs using https://plotdigitizer.com/ (accessed throughout 2025), potentially leading to minor discrepancies between our and the original figures. See Appendix D for details. All computer code and data will be published as a separate archive upon acceptance of this article.

https://doi.org/10.5194/egusphere-2026-4080
Preprint. Discussion started: 21 July 2026


## Appendix A: Spectral cutoff

Here, we will demonstrate analytically how the low- and high wavenumber regions of the $\mathrm{E_{w\theta}}$ integrals modify the $\mathrm{Fr}_h^{-2}$ and $\mathrm{Re_b}^{-1}$ prefactors in the $\tilde{K}_\theta$ scaling Eq. 9.

Based on Sec. 2, we construct $\mathrm{E_{w\theta}}$ piecewise by extending its scaling to small $k$ ($k \ll 1/\ell$) and large $k$ ($k \gg 1/\eta$). To do this, we will impose a continuity condition at $k = 1/\ell$ and $k = 1/\eta$ and apply the cospectrum inequality (O'Gorman and Pullin, 2005)

$$|\mathrm{E_{w\theta}}| \leq \left(\frac{2\mathrm{E_\theta E_u}}{3}\right)^{1/2} \tag{A1}$$

on the energy and scalar variance spectra ($\mathrm{E_u}$ and $\mathrm{E_\theta}$). We then calculate the integral $\int_0^\infty \mathrm{d}k\,\mathrm{E_{w\theta}}$ piecewise.

For the large scales ($k \ll 1/\ell$), we require continuity at $\ell$ ($\mathrm{E_{w\theta}}(k = 1/\ell) = \mathrm{C_{w\theta}}\epsilon^{1/3}\ell^{7/3}$) and use Eq. A1. Then

$$0 < \int\limits_0^{1/\ell} \mathrm{d}k\,\mathrm{E_{w\theta}} \leq \frac{1}{s_a+1}\mathrm{C_{w\theta}}G\epsilon^{1/3}\ell^{4/3}, \tag{A2}$$

where $s_a \in [2,4]$ is the exponent in the large scales, akin to $\mathrm{E_u} \sim k^a$ with $a = 4$ for Batchelor turbulence (Batchelor and Proudman, 1956) or $a = 2$ for Saffman turbulence (Saffman, 1967), and $\mathrm{E_\theta} \sim k^2$ (Chasnov, 1994).

Similarly, in the viscous-convective range $1/\eta < k < 1/\eta_B$ we can assume $\mathrm{E_u} \sim k\exp(-\beta k\eta)$ (Khurshid et al., 2018) and $\mathrm{E_\theta} \sim k^{-1}$ (Batchelor, 1959; Kraichnan, 1968), hence

$$0 < \int\limits_{1/\eta}^{1/\eta_B} \mathrm{d}k\,\mathrm{E_{w\theta}} \leq \mathrm{C_{w\theta}}\frac{2}{\beta}\left(1 - \exp(-\beta/2(\sqrt{\mathrm{Pr}} - 1))\right). \tag{A3}$$

Finally, in the viscous-diffusive range $1/\eta_B \leq k$ both $\mathrm{E_\theta}$ and $\mathrm{E_u}$ decay exponentially; we hence assume $\int_{1/\eta_B}^{\infty} \mathrm{d}k\,\mathrm{E_{w\theta}} \approx 0$.

In sum, Eqs. 8, A2, and A3 yield

$$K_\theta \lesssim \mathrm{C_{w\theta}}\epsilon^{1/3}\left(\left(\frac{3}{4} + \frac{1}{s_a+1}\right)\ell^{4/3} + \left(\frac{2}{\beta}\left(1 - \exp\left(\frac{-\beta(\sqrt{\mathrm{Pr}}-1)}{2}\right)\right) - \frac{3}{4}\right)\eta^{4/3}\right). \tag{A4}$$

With $\mathrm{Pr} \approx 7$ and $\beta \approx 6.7$ (Khurshid et al., 2018), the viscous-convective contribution Eq. A3 is comparatively small. As expected, the largest contribution to Eq. A4 is from the inertial range, the viscous-convective contribution mattering only for $\ell \to \eta$. Crucially, the functional form is the same, the only modifications pertaining to prefactors of $\ell$ and $\eta$.

## Appendix B: Lagrangian statistics

Interestingly, a similar scaling $K_\theta \sim \mathcal{O}\left(\ell^{4/3}\right) - \mathcal{O}\left(\ell^{2/3}\eta^{2/3}\right)$ as in Eq. 8 also arises from an entirely different line of argument. For a Brownian particle in isotropic turbulence with molecular diffusivity $\kappa_\theta$, for times $t > T_L$,

$$K_\theta = \sigma_u^2 T_L, \tag{B1}$$

https://doi.org/10.5194/egusphere-2026-4080
Preprint. Discussion started: 21 July 2026


where $T_L = \int_0^\infty \mathrm{d}\tau R_L(\tau)$ is the decorrelation time of particle velocity $u^+$ along Lagrangian trajectories defined with $\langle u_i^+(t) u_j^+(t+\tau)\rangle \equiv \sigma_u^2 R_L \delta_{ij}$ and $\sigma_u^2$ the velocity variance. From DNS, it is found that $T_L$ with increasing Re very quickly approaches $0.31 T_E$ (Borgas et al., 2004) with the Eulerian time scale $T_E = \sigma_u^2/\epsilon$. With $\sigma_u^2 = \frac{2}{3}\mathrm{K}$ (K the turbulence kinetic energy) we have

$$\sigma_u^2 \approx \frac{2}{3} \int\limits_{1/\ell}^{1/\eta} \mathrm{d}k\, \mathrm{E_u} = \mathrm{C_u} \epsilon^{2/3} \left(\ell^{2/3} - \eta^{2/3}\right) \tag{B2}$$

with $\mathrm{C_u} \approx 1.5$ the Kolmogorov constant for the three-dimensional energy spectrum (Kaneda and Morishita, 2012). Hence

$$K_\theta \simeq 0.31 \sigma_u^4/\epsilon \simeq 0.7 \epsilon^{1/3} \left(\ell^{4/3} - 2\ell^{2/3}\eta^{2/3} + \eta^{4/3}\right) \tag{B3}$$

and

$$\tilde{K}_\theta \approx 0.7 \left(\frac{1}{\mathrm{Fr}^2} - \frac{2}{\mathrm{Fr}\sqrt{\mathrm{Re_b}}} + \frac{1}{\mathrm{Re_b}}\right) = 0.7 \left(\frac{1}{\mathrm{Fr}} - \frac{1}{\sqrt{\mathrm{Re_b}}}\right)^2 \qquad \text{for } \mathrm{Fr} > 1,\, \mathrm{Re_b} > 1 \tag{B4}$$

which strongly resembles Eq. 9. For $\mathrm{Re_b} \gg 1$, both tend to the same scaling $\sim \mathrm{Fr}^{-2}$.

## Appendix C: Glossary

- $\langle\cdot\rangle$: Segment-wise average
- $\beta_S$, $\alpha_T$: saline contraction and thermal expansion coefficients
- $\tilde{K}_\theta$: Nondimensional eddy diffusivity $\tilde{K}_\theta \equiv K_\theta N^2/\epsilon$ of any tracer $\theta$ (Eq. 4)
- $\tilde{K}_\rho$: Nondimensional eddy diffusivity of density or buoyancy $\tilde{K}_\rho \equiv K_\rho N^2/\epsilon$
- $\Gamma$: Mixing coefficient $\Gamma \equiv F_b/\epsilon$
- $\Gamma_\chi$: Mixing coefficient variant $\Gamma_\chi \equiv \epsilon_b/\epsilon$
- $\Gamma_{\mathcal{M}}$: Mixing coefficient variant $\Gamma_{\mathcal{M}} \equiv \mathcal{M}/\epsilon$
- $\mathcal{M}$: Rate of irreversible mixing (Winters et al., 1995)
- $\epsilon$: Turbulence kinetic energy dissipation
- $\epsilon_\theta$, $\epsilon_b$, $\epsilon_T$: Scalar variance dissipation rate of arbitrary tracer $\theta$, buoyancy $b$, temperature $T$
- $k$: Wavenumber
- K: Turbulence kinetic energy

https://doi.org/10.5194/egusphere-2026-4080
Preprint. Discussion started: 21 July 2026


- $K_\theta$, $K_\rho$: Turbulent vertical diffusivity of any tracer $\theta$ or density $\rho$ defined by Eq. 1
- $\kappa_\theta$: Molecular diffusivity of tracer $\theta$ in seawater
- $\nu$: Molecular viscosity of seawater
- $F_b$, $F_\theta$, $F_T$, $F_S$: Vertical turbulent upward flux of buoyancy $b$, tracer $\theta$, temperature $T$, salinity $S$
- $N$: Buoyancy frequency, $N^2 = -g/\rho_0\,\partial\rho/\partial z$
- $b$: Buoyancy, $b = -g\rho'/\rho$ for some density excursion $\rho'$
- Re: Reynolds number $(\ell/\eta)^{4/3}$
- $\mathrm{Re}_*$: $\min(\mathrm{Re}, \mathrm{Re_b})$, used to select the outer wavenumber scale (Ozmidov or integral) depending on whether $\mathrm{Fr}_h < 1$ or $\mathrm{Fr}_h > 1$
- $\mathrm{Re_b}$: Buoyancy Reynolds number $\epsilon/(\nu N^2)$, equivalent to $U\ell/\nu$ when assuming Taylor scaling
- Fr: Froude number $U/(N\ell)$
- $\mathrm{Fr}_h$: Horizontal Froude number $U/(N\ell_h) \simeq \epsilon/(N\mathrm{K})$
- $\mathrm{Fr}_v$: Vertical Froude number $U/(N\ell_v)$
- Pr: Prandtl number $\nu/\kappa_\theta$ (called Schmidt number when the tracer is salinity rather than temperature)
- $\eta$: Kolmogorov length $(\nu^3/\epsilon)^{1/4}$
- $\eta_B$: Batchelor length scale $\eta/\sqrt{\mathrm{Pr}}$
- $\ell_O$: Ozmidov length $(\epsilon/N^3)^{1/2}$
- $\ell_T$: Thorpe length scale based on density reordering (Thorpe, 1977)
- $\ell_E$: Ellison length scale (Smyth et al., 2001)
- $\ell$: Integral (or outer) length scale
- $\ell_h$: Horizontal integral length scale
- $\ell_v$: Vertical integral length scale
- $U$: Turbulence velocity scale. In stratified turbulence, represents the typical horizontal velocity scale corresponding to the largest structures.
- $\sigma_u$: Root mean square turbulent velocity

https://doi.org/10.5194/egusphere-2026-4080
Preprint. Discussion started: 21 July 2026


- $G$: Mean gradient of tracer $\theta$
- $T_L$: Lagrangian decorrelation time scale for Brownian particle
- $T_E$: Eulerian decorrelation time scale
- $s_a$: k exponent of power law in $\mathrm{E_{w\theta}}$ for large scales $k < 1/\ell$
- $s_b$: k exponent of power law in $\mathrm{E_{w\theta}}$ for stratified range $1/\ell \ll k \ll 1/\ell_O$
- $s_c$: k exponent of power law in $\mathrm{E_{w\theta}}$ for inertial-convective range scales
- $\varphi$: Multiple of wavelength for emulating spectral smoothing
- $\mathrm{E_{w\theta}}$: Scalar-velocity cospectrum
- $\mathrm{C_{w\theta}}$: Constant of proportionality of $\mathrm{E_{w\theta}}$ in inertial-convective range, around $1.5$
- $\mathrm{E_\theta}$: Scalar variance spectrum of tracer $\theta$
- $\mathrm{C_\theta}$: Obukhov-Corrsin constant, proportionality factor in inertial-convective range of $\mathrm{E_\theta}$, approximately 0.67 (Sreenivasan, 1996)
- $\mathrm{E_u}$: Turbulent kinetic energy spectrum
- $\mathrm{C_u}$: Kolmogorov constant
- $\phi$: Stability factor $\phi(z/L) = 1 + \gamma z/L$ in Monin-Obukhov similarity
- $\gamma$: Empirical factor in $\phi$, measured to lie between 4 and 8
- $L$: Monin-Obukhov length $L = U^3/(\kappa F_b)$
- $\kappa$: von Kármán constant, $\kappa \approx 0.4$
- $R_{OT}$: Ozmidov-Thorpe length scale ratio $\ell_O/\ell_T \approx \ell_O/\ell_E$
- $\beta$: Exponential rolloff parameter in the viscous subrange of $\mathrm{E_u}$
- $S_0$: Ice-ocean interface salinity
- $S_{\mathrm{ice}}$: Bulk salinity of sea ice, taken as $S_{\mathrm{ice}} = 4$
- $Q_L$: Latent heat of melting sea ice divided by the specific heat of sea water, $Q_L = 73.3\,\mathrm{K}$

https://doi.org/10.5194/egusphere-2026-4080
Preprint. Discussion started: 21 July 2026


## Appendix D: Data sources

Andrea Maffioli kindly provided the forced DNS data of MBL16 (Maffioli et al., 2016). Eddy covariance data from PFMR17 (Peterson et al., 2017) were retrieved from personal archives with kind support from Ilker Fer. The regression coefficients of $\tilde{K}_\theta$ against $\mathrm{Re_b}$ of BB13 were retrieved from the paper (Bouffard and Boegman, 2013). All other data reported in the literature were unattainable in digital format and hence were visually scraped from the published graphs using https://plotdigitizer.com/, specifically:

- SMC01 (Smyth et al., 2001), DNS of breaking Kelvin-Helmholtz billows: Fig. 15 provided $\Gamma$ vs. $\frac{\ell_O}{\ell_E^{3/4}\ell_T^{1/4}}$.
- SMC01 (Smyth et al., 2001), observational data: Fig. 14 provided a visual log-log regression of $\Gamma$ on $\frac{\ell_O}{\ell_E^{3/4}\ell_T^{1/4}}$.
- SKIF05 (Shih et al., 2005): Fig. 11 provided the relation between $\mathrm{Re_b}$ and $\mathrm{Fr}_h$ with $\mathrm{K} = q^2/2$ and $\mathrm{Fr}_h = \epsilon/(N\mathrm{K})$. Fig. 1 of Garanaik and Venayagamoorthy (2019) provided $\Gamma$ vs $\mathrm{Fr}_h$.
- GV19 (Garanaik and Venayagamoorthy, 2019): Fig. 1 provided $\Gamma$ vs $\mathrm{Fr}_h$. Fig. 2 provided $\Gamma$ vs $\mathrm{Re_b}$. Fig. 3 provided the piecewise linear (log-log) relationship between $\mathrm{Fr}_h$ and $\frac{\ell_O}{\ell_T}$ used throughout this paper, always assuming $\ell_E \simeq \ell_T$ (Mater et al., 2013). Fig. 4 provided the relationship between $\Gamma$ and $\frac{\ell_O}{\ell_T}$ for SKIF05, MBL16, and GV19.
- IH18 (Ijichi and Hibiya, 2018): Fig. 8 provided $\Gamma$ vs. $\frac{\ell_O}{\ell_T}$ for $\mathrm{Re_b} \geq 40$.

*Author contributions.* Randelhoff: Conceptualization, Methodology, Visualization, Software, Data curation, Writing- Original draft preparation, Reviewing and Editing

*Competing interests.* The author declares no competing interests.

*Acknowledgements.* This study was supported by the TURBOT project (Research Council of Norway grant 352188). We thank two anonymous reviewers and Ilker Fer for comments which helped improve a first version of this manuscript.

https://doi.org/10.5194/egusphere-2026-4080
Preprint. Discussion started: 21 July 2026


## References

Batchelor, G. K.: Small-Scale Variation of Convected Quantities like Temperature in Turbulent Fluid Part 1. General Discussion and the Case of Small Conductivity, Journal of Fluid Mechanics, 5, 113, https://doi.org/10.1017/S002211205900009X, 1959.

Batchelor, GK. and Proudman, I.: The Large-Scale Structure of Homogenous Turbulence, Philosophical Transactions of the Royal Society of London. Series A, Mathematical and Physical Sciences, 248, 369–405, https://doi.org/10.1098/rsta.1956.0002, 1956.

Borgas, M. S., Sawford, B. L., Xu, S., Donzis, D. A., and Yeung, P. K.: High Schmidt Number Scalars in Turbulence: Structure Functions and Lagrangian Theory, Physics of Fluids, 16, 3888–3899, https://doi.org/10.1063/1.1780550, 2004.

Bos, W. J. T., Touil, H., Shao, L., and Bertoglio, J.-P.: On the Behavior of the Velocity-Scalar Cross Correlation Spectrum in the Inertial Range, Physics of Fluids, 16, 3818–3823, https://doi.org/10.1063/1.1779229, 2004.

Bos, W. J. T., Touil, H., and Bertoglio, J.-P.: Reynolds Number Dependency of the Scalar Flux Spectrum in Isotropic Turbulence with a Uniform Scalar Gradient, Physics of Fluids, 17, 125 108, https://doi.org/10.1063/1.2140848, 2005.

Bouffard, D. and Boegman, L.: A Diapycnal Diffusivity Model for Stratified Environmental Flows, Dynamics of Atmospheres and Oceans, 61–62, 14–34, https://doi.org/10.1016/j.dynatmoce.2013.02.002, 2013.

Brethouwer, G., Billant, P., Lindborg, E., and Chomaz, J.-M.: Scaling Analysis and Simulation of Strongly Stratified Turbulent Flows, Journal of Fluid Mechanics, 585, 343–368, https://doi.org/10.1017/s0022112007006854, 2007.

Caulfield, C. P.: Layering, Instabilities, and Mixing in Turbulent Stratified Flows, Annual Review Fluid Mechanics, 53, 113–145, https://doi.org/10.1146/annurev-fluid-042320-100458, 2020.

Caulfield, C. P. and Peltier, W. R.: The Anatomy of the Mixing Transition in Homogeneous and Stratified Free Shear Layers, Journal of Fluid Mechanics, 413, 1–47, https://doi.org/10.1017/S0022112000008284, 2000.

Chasnov, J. R.: Similarity States of Passive Scalar Transport in Isotropic Turbulence, Physics of Fluids, 6, 1036–1051, https://doi.org/10.1063/1.868337, 1994.

Davidson, P. A.: Turbulence in Rotating, Stratified and Electrically Conducting Fluids, Cambridge University Press, 1 edn., ISBN 978-1-139-20867-3 978-1-107-02686-5, https://doi.org/10.1017/CBO9781139208673, 2013.

Dillon, T. M.: Vertical Overturns: A Comparison of Thorpe and Ozmidov Length Scales, Journal of Geophysical Research, 87, 9601, https://doi.org/10.1029/jc087ic12p09601, 1982.

Garanaik, A. and Venayagamoorthy, S. K.: Assessment of Small-Scale Anisotropy in Stably Stratified Turbulent Flows Using Direct Numerical Simulations, Physics of Fluids, 30, 126 602, https://doi.org/10.1063/1.5055871, 2018.

Garanaik, A. and Venayagamoorthy, S. K.: On the Inference of the State of Turbulence and Mixing Efficiency in Stably Stratified Flows, Journal of Fluid Mechanics, 867, 323–333, https://doi.org/10.1017/jfm.2019.142, 2019.

Gargett, A. E. and Moum, J. N.: Mixing Efficiencies in Turbulent Tidal Fronts: Results from Direct and Indirect Measurements of Density Flux, Journal of Physical Oceanography, 25, 2583–2608, https://doi.org/10.1175/1520-0485(1995)025<2583:MEITTF>2.0.CO;2, 1995.

Gotoh, T. and Yeung, P.: Passive Scalar Transport in Turbulence: A Computational Perspective, in: Ten Chapters in Turbulence, edited by Davidson, P. A., Kaneda, Y., and Sreenivasan, K. R., pp. 87–131, Cambridge University Press, 1 edn., ISBN 978-0-521-76944-0 978-1-139-03281-0, https://doi.org/10.1017/CBO9781139032810.004, 2012.

Gregg, M., D'Asaro, E., Riley, J., and Kunze, E.: Mixing Efficiency in the Ocean, Annual Review of Marine Science, 10, 443–473, https://doi.org/10.1146/annurev-marine-121916-063643, 2018.

https://doi.org/10.5194/egusphere-2026-4080
Preprint. Discussion started: 21 July 2026


Holloway, G.: Considerations on the Theory of Temperature Spectra in Stably Stratified Turbulence, Journal of Physical Oceanography, 16, 2179–2183, https://doi.org/10.1175/1520-0485(1986)016<2179:COTTOT>2.0.CO;2, 1986.

Ijichi, T. and Hibiya, T.: Observed Variations in Turbulent Mixing Efficiency in the Deep Ocean, Journal of Physical Oceanography, 48, 1815–1830, https://doi.org/10.1175/JPO-D-17-0275.1, 2018.

Ivey, G. N. and Imberger, J.: On the Nature of Turbulence in a Stratified Fluid. Part I: The Energetics of Mixing, Journal of Physical Oceanography, 21, 650–658, https://doi.org/10.1175/1520-0485(1991)021<0650:OTNOTI>2.0.CO;2, 1991.

Kaimal, J. C.: Turbulence Spectra, Length Scales and Structure Parameters in the Stable Surface Layer, Boundary-Layer Meteorology, 4, 289–309, https://doi.org/10.1007/BF02265239, 1973.

Kaneda, Y. and Morishita, K.: Small-Scale Statistics and Structure of Turbulence – in the Light of High Resolution Direct Numerical Simulation, in: Ten Chapters in Turbulence, edited by Davidson, P. A., Kaneda, Y., and Sreenivasan, K. R., pp. 1–42, Cambridge University Press, Cambridge, 2012.

Khurshid, S., Donzis, D. A., and Sreenivasan, K. R.: Energy Spectrum in the Dissipation Range, Physical Review Fluids, 3, 082 601, https://doi.org/10.1103/PhysRevFluids.3.082601, 2018.

Klema, M. R. and Venayagamoorthy, S. K.: Mixing Rates in Stably Stratified Flows with Respect to the Turbulent Froude Number and Turbulent Scales, Environmental Fluid Mechanics, 23, 1037–1049, https://doi.org/10.1007/s10652-023-09925-1, 2023.

Kraichnan, R. H.: Small-Scale Structure of a Scalar Field Convected by Turbulence, The Physics of Fluids, 11, 945–953, https://doi.org/10.1063/1.1692063, 1968.

Ledwell, J. R., Watson, A. J., and Law, C. S.: Mixing of a Tracer in the Pycnocline, Journal of Geophysical Research: Oceans, 103, 21 499–21 529, https://doi.org/10.1029/98JC01738, 1998.

Ledwell, J. R., Montgomery, E. T., Polzin, K. L., St. Laurent, L. C., Schmitt, R. W., and Toole, J. M.: Evidence for Enhanced Mixing over Rough Topography in the Abyssal Ocean, Nature, 403, 179–182, https://doi.org/10.1038/35003164, 2000.

Lewis, M. R., Hebert, D., Harrison, W. G., Platt, T., and Oakey, N. S.: Vertical Nitrate Fluxes in the Oligotrophic Ocean, Science, 234, 870–873, https://doi.org/10.1126/science.234.4778.870, 1986.

Lienhard V, J. H. and Van Atta, C. W.: The Decay of Turbulence in Thermally Stratified Flow, Journal of Fluid Mechanics, 210, 57–112, https://doi.org/10.1017/S0022112090001227, 1990.

Lumley, J.: The Spectrum of Nearly Inertial Turbulence in a Stably Stratified Fluid, Journal of the Atmospheric Sciences, 21, 99–102, https://doi.org/10.1175/1520-0469(1964)021<0099:TSONIT>2.0.CO;2, 1964.

Maffioli, A. and Davidson, P. A.: Dynamics of Stratified Turbulence Decaying from a High Buoyancy Reynolds Number, Journal of Fluid Mechanics, 786, 210–233, https://doi.org/10.1017/jfm.2015.667, 2016.

Maffioli, A., Brethouwer, G., and Lindborg, E.: Mixing Efficiency in Stratified Turbulence, Journal of Fluid Mechanics, 794, R3, https://doi.org/10.1017/jfm.2016.206, 2016.

Mashayek, A., Salehipour, H., Bouffard, D., Caulfield, C. P., Ferrari, R., Nikurashin, M., Peltier, W. R., and Smyth, W. D.: Efficiency of Turbulent Mixing in the Abyssal Ocean Circulation, Geophysical Research Letters, 44, 6296–6306, https://doi.org/10.1002/2016GL072452, 2017.

Mashayek, A., Caulfield, C., and Alford, M.: Goldilocks Mixing in Oceanic Shear-Induced Turbulent Overturns, Journal of Fluid Mechanics, 928, A1, https://doi.org/10.1017/jfm.2021.740, 2021.

Mater, B. D. and Venayagamoorthy, S. K.: The Quest for an Unambiguous Parameterization of Mixing Efficiency in Stably Stratified Geophysical Flows, Geophysical Research Letters, 41, 4646–4653, https://doi.org/10.1002/2014GL060571, 2014.

https://doi.org/10.5194/egusphere-2026-4080
Preprint. Discussion started: 21 July 2026


Mater, B. D., Schaad, S. M., and Venayagamoorthy, S. K.: Relevance of the Thorpe Length Scale in Stably Stratified Turbulence, Physics of Fluids, 25, 076 604, https://doi.org/10.1063/1.4813809, 2013.

McPhee, M.: Air-Ice-Ocean Interaction: Turbulent Ocean Boundary Layer Exchange Processes, Springer New York, https://doi.org/10.1007/978-0-387-78335-2, 2008.

McPhee, M. G. and Martinson, D. G.: Turbulent Mixing Under Drifting Pack Ice in the Weddell Sea, Science, 263, 218–221, https://doi.org/10.1126/science.263.5144.218, 1994.

Meyer, A., Fer, I., Sundfjord, A., and Peterson, A. K.: Mixing Rates and Vertical Heat Fluxes North of Svalbard from Arctic Winter to Spring, Journal of Geophysical Research: Oceans, 122, 4569–4586, https://doi.org/10.1002/2016JC012441, 2017.

Monismith, S. G., Koseff, J. R., and White, B. L.: Mixing Efficiency in the Presence of Stratification: When Is It Constant?, Geophysical Research Letters, 45, 5627–5634, https://doi.org/10.1029/2018GL077229, 2018.

Moum, J. N.: Efficiency of Mixing in the Main Thermocline, Journal of Geophysical Research: Oceans, 101, 12 057–12 069, https://doi.org/10.1029/96JC00508, 1996.

Munk, W. and Wunsch, C.: Abyssal Recipes II: Energetics of Tidal and Wind Mixing, Deep Sea Research Part I: Oceanographic Research Papers, 45, 1977–2010, https://doi.org/10.1016/S0967-0637(98)00070-3, 1998.

Mydlarski, L.: Mixed Velocity–Passive Scalar Statistics in High-Reynolds-number Turbulence, Journal of Fluid Mechanics, 475, 173–203, https://doi.org/10.1017/S0022112002002756, 2003.

Mydlarski, L. and Warhaft, Z.: Passive Scalar Statistics in High-Péclet-number Grid Turbulence, Journal of Fluid Mechanics, 358, 135–175, https://doi.org/10.1017/S0022112097008161, 1998.

Nash, J. D. and Moum, J. N.: Estimating Salinity Variance Dissipation Rate from Conductivity Microstructure Measurements, Journal of Atmospheric and Oceanic Technology, 16, 263–274, https://doi.org/10.1175/1520-0426(1999)016<0263:ESVDRF>2.0.CO;2, 1999.

Oakey, N. S.: Determination of the Rate of Dissipation of Turbulent Energy from Simultaneous Temperature and Velocity Shear Microstructure Measurements, Journal of Physical Oceanography, 12, 256–271, https://doi.org/10.1175/1520-0485(1982)012<0256:DOTROD>2.0.CO;2, 1982.

Obukhov, A. M.: Turbulence in an Atmosphere with a Non-Uniform Temperature, Boundary-Layer Meteorology, 2, 7–29, https://doi.org/10.1007/BF00718085, 1971.

O'Gorman, P. A. and Pullin, D. I.: The Velocity-Scalar Cross Spectrum of Stretched Spiral Vortices, Physics of Fluids, 15, 280–291, https://doi.org/10.1063/1.1527916, 2003.

O'Gorman, P. A. and Pullin, D. I.: Effect of Schmidt Number on the Velocity–Scalar Cospectrum in Isotropic Turbulence with a Mean Scalar Gradient, Journal of Fluid Mechanics, 532, 111–140, https://doi.org/10.1017/S0022112005003903, 2005.

Osborn, T. R.: Estimates of the Local Rate of Vertical Diffusion from Dissipation Measurements, J. Phys. Oceanogr., 10, 83–89, https://doi.org/10.1175/1520-0485(1980)010<0083:EOTLRO>2.0.CO;2, 1980.

Osborn, T. R. and Cox, C. S.: Oceanic Fine Structure, Geophysical Fluid Dynamics, 3, 321–345, https://doi.org/10.1080/03091927208236085, 1972.

Peltier, W. R. and Caulfield, C. P.: MIXING EFFICIENCY IN STRATIFIED SHEAR FLOWS, Annual Review of Fluid Mechanics, 35, 135–167, https://doi.org/10.1146/annurev.fluid.35.101101.161144, 2003.

Peters, H., Gregg, M. C., and Sanford, T. B.: Detail and Scaling of Turbulent Overturns in the Pacific Equatorial Undercurrent, Journal of Geophysical Research: Oceans, 100, 18 349–18 368, https://doi.org/10.1029/95JC01360, 1995.

https://doi.org/10.5194/egusphere-2026-4080
Preprint. Discussion started: 21 July 2026


Peterson, A. K., Fer, I., McPhee, M. G., and Randelhoff, A.: Turbulent Heat and Momentum Fluxes in the Upper Ocean under Arctic Sea Ice, Journal of Geophysical Research: Oceans, 122, 1439–1456, https://doi.org/10.1002/2016JC012283, 2017.

Pond, S., Phelps, G. T., Paquin, J. E., McBean, G., and Stewart, R. W.: Measurements of the Turbulent Fluxes of Momentum, Moisture and Sensible Heat over the Ocean, Journal of the Atmospheric Sciences, 28, 901–917, https://doi.org/10.1175/1520-0469(1971)028<0901:MOTTFO>2.0.CO;2, 1971.

Riley, J. J. and deBruynKops, S. M.: Dynamics of Turbulence Strongly Influenced by Buoyancy, Physics of Fluids, 15, 2047–2059, https://doi.org/10.1063/1.1578077, 2003.

Riley, J. J. and Lindborg, E.: Recent Progress in Stratified Turbulence, in: Ten Chapters in Turbulence, edited by Davidson, P. A., Kaneda, Y., and Sreenivasan, K. R., pp. 269–317, Cambridge University Press, 1 edn., ISBN 978-0-521-76944-0 978-1-139-03281-0, https://doi.org/10.1017/CBO9781139032810.008, 2012.

Saffman, P. G.: The Large-Scale Structure of Homogeneous Turbulence, Journal of Fluid Mechanics, 27, 581–593, https://doi.org/10.1017/S0022112067000552, 1967.

Salehipour, H. and Peltier, W. R.: Diapycnal Diffusivity, Turbulent Prandtl Number and Mixing Efficiency in Boussinesq Stratified Turbulence, Journal of Fluid Mechanics, 775, 464–500, https://doi.org/10.1017/jfm.2015.305, 2015.

Scotti, A. and White, B.: The Mixing Efficiency of Stratified Turbulent Boundary Layers, Journal of Physical Oceanography, 46, 3181–3191, https://doi.org/10.1175/JPO-D-16-0095.1, 2016.

Shih, L. H., Koseff, J. R., Ivey, G. N., and Ferziger, J. H.: Parameterization of Turbulent Fluxes and Scales Using Homogeneous Sheared Stably Stratified Turbulence Simulations, Journal of Fluid Mechanics, 525, 193–214, https://doi.org/10.1017/S0022112004002587, 2005.

Smyth, W. D., Moum, J. N., and Caldwell, D. R.: The Efficiency of Mixing in Turbulent Patches: Inferences from Direct Simulations and Microstructure Observations, Journal of Physical Oceanography, 31, 1969–1992, https://doi.org/10.1175/1520-0485(2001)031<1969:TEOMIT>2.0.CO;2, 2001.

Sreenivasan, K. R.: The Passive Scalar Spectrum and the Obukhov–Corrsin Constant, Physics of Fluids, 8, 189–196, https://doi.org/10.1063/1.868826, 1996.

Thorpe, S.: Turbulence and Mixing in a Scottish Loch, Philosophical Transactions of the Royal Society of London. Series A, Mathematical and Physical Sciences, 286, 125–181, https://doi.org/10.1098/rsta.1977.0112, 1977.

Watanabe, T. and Gotoh, T.: Scalar Flux Spectrum in Isotropic Steady Turbulence with a Uniform Mean Gradient, Physics of Fluids, 19, 121 701, https://doi.org/10.1063/1.2821906, 2007.

Winters, K. B., Lombard, P. N., Riley, J. J., and D'Asaro, E. A.: Available Potential Energy and Mixing in Density-Stratified Fluids, Journal of Fluid Mechanics, 289, 115–128, https://doi.org/10.1017/S002211209500125X, 1995.